OPTIMIZING MIXING IN THE DILUTION SYSTEM OF A PAPER MACHINE

A Thesis
Presented to
The Academic Faculty

by

Joseph Steele

In Partial Fulfillment
of the Requirements for the Degree
Masters of Paper Science and Engineering in the
School of Mechanical Engineering

Georgia Institute of Technology
May 2010

OPTIMIZING MIXING IN THE DILUTION SYSTEM OF A PAPER MACHINE

Approved by:

Dr. Cyrus Aidun, Advisor
School of Mechanical Engineering
Georgia Institute of Technology

Dr. Marc Smith
School of Mechanical Engineering
Georgia Institute of Technology

Dr. S. Mostafa Ghiaasiaan
School of Mechanical Engineering
Georgia Institute of Technology

Date Approved: January 15, 2010

TABLE OF CONTENTS

LIST OF TABLES

LIST OF FIGURES

LIST OF SYMBOLS AND ABBREVIATIONS

l_m	jet momentum length
q	volumetric flow rate
ρ	density of fluid
ρ_p	density of the injected particles
u_i	fluid velocity in a given direction i
μ	dynamic viscosity of the fluid
p	pressure of the fluid
$\bar{p}$	average pressure of the fluid
g	the force of gravity
A	area
u'	turbulent velocity fluctuation
k	turbulent kinetic energy
ϵ	dissipation rate
F_D	drag force on an injected particle
F_{pr}	force of the pressure gradient on an injected particle
c	concentration of the injected particles
$\bar{c}$	average concentration of the injected particle
$\dot{m}$	mass flow rate of the injected particles
t	residence time of the injected particles
V_c	volume of the cell containing the injected particles
M	second moment of concentration of the injected particles
N	number of cells at a selected surface
CD	Cross Direction

MD	Machine Direction
k- ε	k-epsilon
RSM	Reynold's stress method
DPM	Discrete phase model

SUMMARY

In the flow distribution section of a paper machine, known as the *head box*, water is injected into the fiber suspension (stock) flow through a tee-mixer for more uniform production. This dilution process has two important requirements that must be fulfilled: (1) sufficient mixing so that the dilution flow spreads across the suspension flow and (2) that the injection flow rate not be so large to significantly alter the local head box flow rate. The objective of this research was to find a combination of velocity ratio and tee mixer geometry that lead to the injection flow being well mixed into the stock flow, but at the same time, the injection should not cause the total flow rate to change by more than 1%. Velocity ratios of 0.25, 0.75, 1.33, 1.5 and 2.25 were examined for four different cases of tee mixer geometries using the CFD software Fluent. Two of the cases had added contractions located near the injection point, while the other two cases had a more standard geometry with no added complexities. The pressure drop across the injection point was also measured. Mixing was qualitatively measured by simulating the injection of a passive tracer into the dilution flow. All of the results indicated that the case where the contraction was located after the injection showed the most promising results with quality mixing and lower flow rates. The cases without added contractions showed poor mixing for lower velocity ratios, and for higher velocity ratios, the flow rates were too large. The cases with contractions showed similar mixing, but the outlet flow rates produced were lower when the contraction was located after the injection instead of before it. A velocity ratio of 0.25-0.75 for the mixers with contractions produced acceptable flow rates and sufficient mixing. The simulations also showed that the static

pressure for the contraction cases were nearly identical throughout the majority of the pipe. For both contraction cases the pressure drop across the injection increased with increasing injection flow rate. When the contraction was located before the injection, a pressure drop of 16% was calculated. A pressure drop of 18% to 20% across the injection resulted when the contraction was located after the injection.

CHAPTER 1

INTRODUCTION

Turbulent mixers are widely used today in many different industries from chemical mixing to paper production. In paper manufacturing, local basis weight distribution is one of the most important properties that must be controlled since it describes the uniformity of the paper sheet. Basis weight is defined as the ratio of the mass of the sheet of paper to its area. Because the paper thickness is difficult to quickly measure, basis weight is used to implicitly describe it. An increase in basis weight can therefore imply an increase in the paper thickness. A non-uniform sheet must be avoided since not only does it waste pulp, but perhaps more importantly, the paper sheet may not meet a customer's demands. The basis weight of the final paper product is directly related to the flow rate of the pulp mixture running through the paper machine. Because of the importance of a uniform sheet, the basis weight is controlled in two directions: the machine direction (MD) and the cross direction (CD). The machine direction is parallel to the direction pulp is processed through the machine, and the cross direction is the transverse direction and perpendicular to the machine direction. One of the methods for controlling basis weight is by locally diluting the pulp mixture, also called the stock flow, with water in either the machine or cross direction. This dilution control occurs in the head box of a paper machine. In general a paper machine takes in wet pulp, and through various mechanical processes, creates a final product in the form of dry rolls of paper. The process is commonly divided into sections known as the wet end and dry end. Pulp entering the wet end of the machine usually consists of around 99% water. The goal of

the wet end is to reduce the water in the pulp and to form the fiber webs into an even wet sheet. The dry end of the machine then further reduces the water in the wet sheet to under 1% and adds final coatings if desired.

For this study, the wet end is the most relevant part of the machine. The wet end can be divided into three main sections: the head box, former, and the press. The purpose of the head box is to uniformly distribute the pulp onto the forming tray where the actual paper sheet is formed. The goal of the head box is then to mix the fiber water suspension so that the fibers have a homogenous distribution across the width of the machine. The head box is comprised of a tapered section that feeds the stock flow through a bank of several hundred identical tubes. The tapered section and tube bank are used to create turbulence and to evenly divide the flow. Turbulence is generated to disperse clumps in the fiber which would cause a non-uniform final product. Furthermore dilution water can be pumped into each individual tube in order to control the amount of fibers flowing through that tube. The head box then delivers the stock flow to the wire tray, which appears like a conveyor belt covered with a mesh cloth, in the forming section. The former is where the fibers are shaped into a paper sheet and where drainage begins. From the former, the sheet is then processed into the pressing section before moving to the dry end.

In the head box of a paper machine, dilution flow is injected into the stock flow through a tee-mixer for CD basis weight control. The basis weight of the paper sheet is measured at several points across the width of the sheet at the end of the paper machine. Some variation in basis weight is expected, but if the basis weight is determined to be too large or too small at one point on the sheet, then the dilution flow in the head box is

adjusted to alleviate this problem. If the basis weight is too high at one point, then the dilution flow is increased in the corresponding section in tube bank of the head box. The result of this that since flow rate through the head box is kept constant, the stock flow in that section of the head box is reduced and the fiber to water ratio in that tube of the head box is reduced. The total flow rate, stock plus dilution, exiting the head box is kept constant in order to maintain a uniform product. Because fewer fibers are now flowing to that particular section, the local basis weight at that point in the sheet will drop to the desired level. This dilution flow usually consists of excess water collected from the former drainage trays injected at 5% to 15% of the stock flow rate. The dilution process has two important requirements that must be fulfilled: (1) sufficient mixing so that the dilution flow spreads across the stock flow and (2) that the injection flow rate not be so large to significantly alter the local head box flow rate. The ratio of the injected dilution flow rate to the main stock flow rate is known as the velocity ratio. An important consideration is that the impact of the injection on the head box flow depends on flow resistances present in the system. Different styles of head boxes will produce different flow resistances upstream and downstream. Therefore it is necessary to test different tee-mixer geometries that will produce varying flow resistance.

Research Objectives

The objective of this research is to find a combination of velocity ratio and tee mixer geometry that leads to the injection flow being well mixed into the stock flow, but at the same time, the injection should not cause the total flow rate to change by more than 1%. Since the main inlet conditions were fixed, altering velocity ratio actually

demonstrates the impact of the increased injection flow rate on the system. Furthermore the geometry of the tee-junction is specifically varied by adjusting the location of the injection tee and adding contractions in the main pipe. The contractions are added to increase flow resistance and to study their effect on mixing. Velocity ratios of 0.25, 0.75, 1.33, 1.5 and 2.25 were examined for four different cases of tee mixer geometries as shown in Figures 1.1-1.4. The dimensions of Table 1.1 and the diagrams shown in Figures 1.1-1.4 were provided by Dr. Jay Shands of Johnson Foils (personal communication, August 2008). Cases 3 and 4, shown in Figures 1.3 and 1.4 respectively, use the same cross section and injection pipe location as case 1 shown in Figure 1.2. The values for the dimensions shown in Figures 1.1-1.4 are presented in Table 1.1. The variables *d* represent the various diameters shown in Figures 1.1-1.4, and *l* is the length of the contractions. These contractions are circular and connected to the walls of the pipe. In Figures 1.1-1.4, *u* and *v* are fluid velocities. Mixing is judged by examining the concentration and trajectories of a simulated tracer injected into the tee junction. Flow rates are measured at both the inlet and outlet of the tee mixer so that the change in flow rate can be calculated. Simulations were conducted using both the k-epsilon and Reynold's stress models. Pressure drops across the injection point were also measured.

Table 1.1: Dimensions for the actual dilution system

Dimensions	Values	Units
d_p	60	mm
d_i	16	mm
d_1	42	mm
d_2	35	mm
x	18	mm
d_o	42	mm
l	25	mm

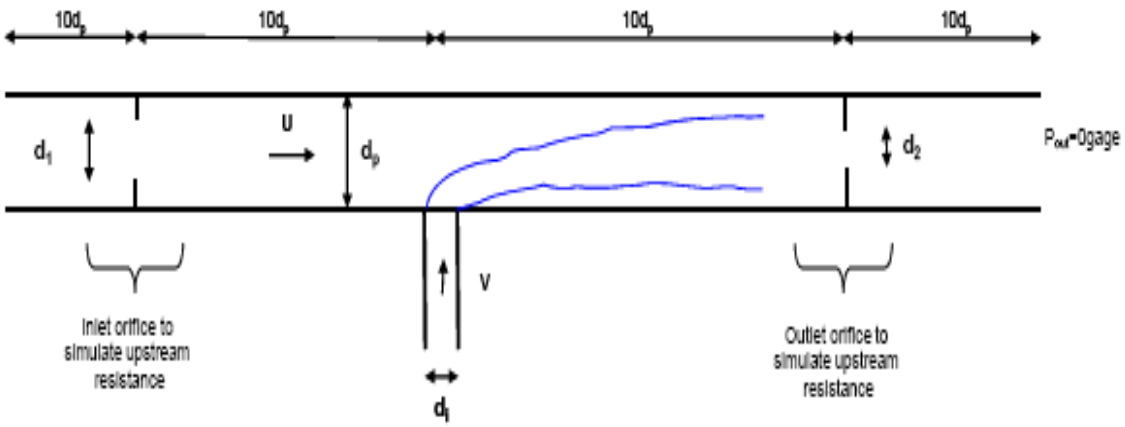

Figure 1.1: Two dimensional diagram of tee junction for modeling cases 1 and 2.

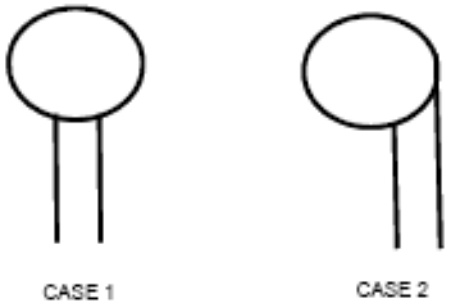

Figure 1.2: Cross sectional view of tee junction for modeling cases 1 and 2.

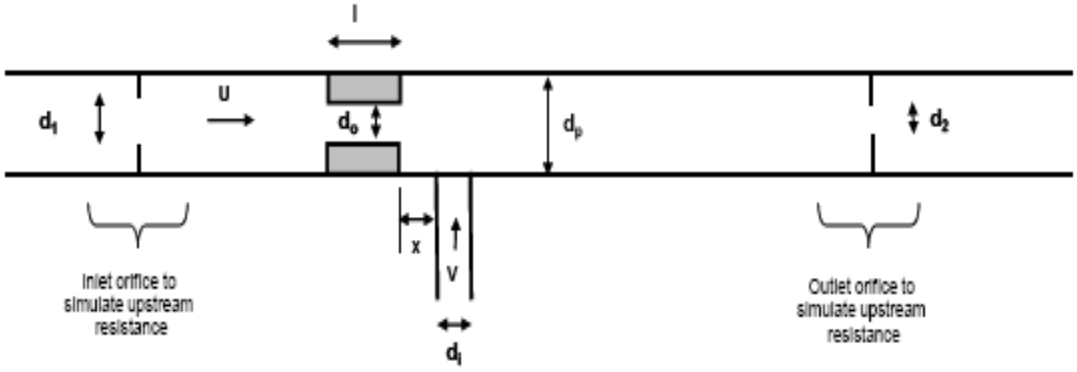

Figure 1.3: Two dimensional diagram of the tee junction for modeling for case 3.

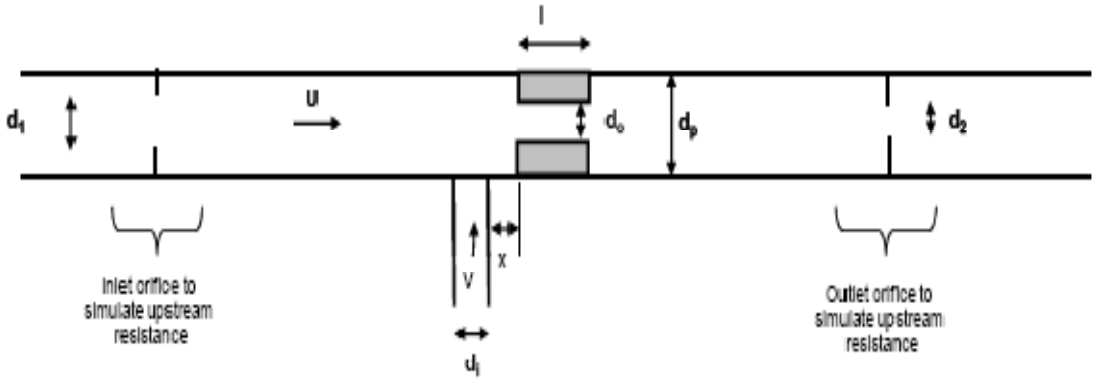

Figure 1.4: Two dimensional diagram of the tee junction for modeling for case 4.

CHAPTER 2

BACKGROUND

Turbulent mixers are used in many industries including chemical production, combustion reactors, and paper production. In 1930, Chilton and Genereuax used smoke visualization to determine that a right angle was necessary for rapid tee mixing in pipes. Furthermore they found that with velocity ratios of 2 to 3, the injected flow had completely dispersed across the diameter of the pipe within 3 pipe diameters. Since then injecting a secondary fluid at right angle into a turbulent flow has been used as a simple method for efficient mixing.

One historically used method for quantitatively measuring the quality of the mixing is by computing the second moment of concentration of a tracer injected into the flow. The second moment is also known as the standard deviation which is a measurement of the spread of a set from an average value. In this case, the second moment of concentration measures the degree to which the concentration of the tracer changes across the diameter of the pipe. A lower second moment is equivalent to a well-mixed state since a near-zero second moment shows that the concentration across the diameter is nearly identical. Forney and Sroka (1989) in examining tee mixers assumed that the mixing could be divided into two sections. For several pipe diameters near the injection point, mixing is controlled by the turbulence of the jet. Downstream the injected flow is assumed to move parallel to the centerline of the pipe with mixing controlled by diffusion. An example of the tee-junction used by Forney and Sroka (1989) in their studies is shown in Figure 2.1.

In order to further characterize the regions of mixing, Forney and Sroka (1989) defined the dimensionless parameter known as the jet momentum length as the distance the injected jet penetrates into the flow before bending into the main flow. The jet momentum (l_m) is defined as the product of the velocity ratio (r) and injection pipe diameter (d). Furthermore they found a similarity solution to describe the second moment of concentration as a function of distance. This solution predicted that the second moment would decrease according to the power law of $(x/D)^{-4/3}$, where D is the main pipe diameter and x is horizontal distance downstream from the injection point. This solution was found to agree well with experimental data. Several conditions for the jet momentum length (l_m) were also found. If $l_m/D < 0.07$, then the maximum tracer concentration and jet centerline are found near the wall of the injection point. This causes the jet to just act as a wall source. When $0.07 < l_m/D < 1.0$, then the second moment of concentration decreases proportionally to $(l_m/D)^{-2}$. This predicts that the maximum tracer concentration moves closer towards the opposite wall from the injection point with increasing jet momentum. When $l_m/D > 1.0$, the jet impinges on the opposite wall from the injection point. Finally for $l_m/D < 1.0$, experimental data showed that the second moment of concentration decreased downstream according the 4/3 power law as predicted by the similarity solution. However when the jet impinges on the opposite pipe wall, $l_m/D > 1.0$, the data does not follow the 4/3 power law.

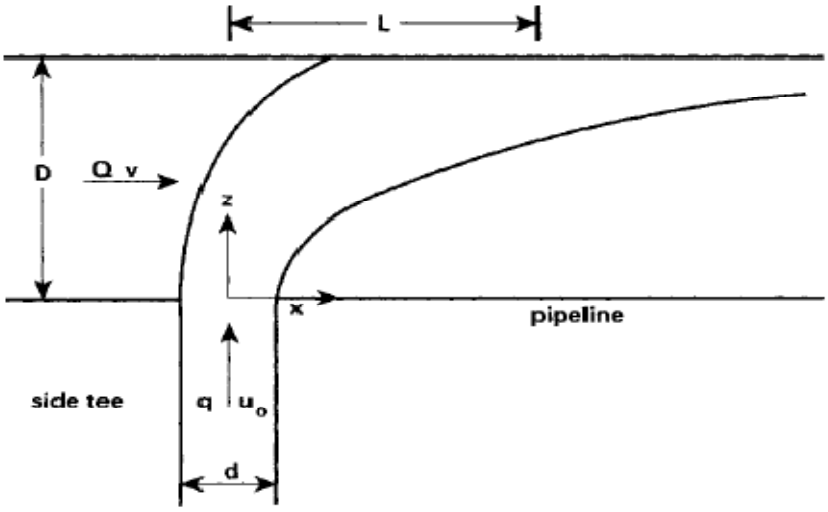

Figure 2.1: Diagram of a tee-mixer as used by Forney and Sroka.

Forney and Gray (1990) later investigated jet impingement and fast turbulent mixers where mixing occurred within the first three pipe diameters. In their study, they found an equation that describes where the point of jet impingement on the opposite wall occurs downstream from injection based on the main and injection pipe diameters and velocity ratio. This equation was found to be accurate to within 3% of experimental data. Busko and Cozewith (1989) also studied mixing in the first three pipe diameters. With increasing velocity ratio, it was found that the jet penetrated farther into the cross flow before bending. Velocity ratios that positioned the jet along the pipe centerline were found for several diameter ratios. All of these velocity ratios were greater than 2, and at a high enough velocity ratio, the jet impinged on the opposite wall. This study used a colored tracer injected into a fluid to perform mixing experiments with the mixing length defined as the length downstream measured from the injection point where the color of the tracer disappeared. The minimal mixing length was found over a range of velocity ratios rather than one distinct value. Furthermore, the mixing length would eventually

increase past the minimum length with increasing velocity ratio. Impingement though did not improve mixing, but rather increased the required mixing length. Therefore Busko and Cozewith concluded that the optimum range of velocity ratios corresponded to the jet being centered along the pipe centerline.

The effect of Reynolds (Re) number on mixing length was also studied. For Re > 10,000, the mixing length was found to be independent of Reynolds number.

Meng and Pan (2001) further studied mixing in the near field of a tee mixer using non-intrusive laser based experimental techniques in order to provide validation and insight into existing CFD models used for tee mixers. In the near field, less than 2 pipe diameters, it was assumed that turbulent dispersion dominates the flow in a tee mixer while diffusion dominates the flow after 3 pipe diameters. Velocity ratios of 3.06 and 5.04 were studied within the jet mixing regime where $0.07 < l_m/D < 1.0$. Velocity ratios that cause jet impingement on the pipe wall were not examined since this creates undesired stresses on the walls. Also for $l_m/D < 0.07$, the mixing is poor and was therefore not studied. The flow structure for these two velocity ratios was visualized and described in terms of five vortical structures that are shown in Figure 2.2: the jet shear layer with Kelvin-Helmholz vortices, the counter-rotating vortex pair that comes from the jet once the jet bends into the main flow, the wake structures behind the jet, the horseshoe vortices upstream of the injection point, and the hanging vortex. The jet shear layer was found to be present on the upper half of the jet with a roll-up of the shear layer in the spanwise direction. The visible rolled up vortices are responsible for entraining the main flow into the jet. Although the counter-rotating vortex pairs (CVP) could not be visualized, evidence of their existence was found to be present in statistical data of the

flow. The data suggests that the CVP is responsible for the injection jet expansion. Hanging vortices were apparent in all of the visualizations and were shown to be responsible for both creating the CVP and causing upward motion in the jet downstream.

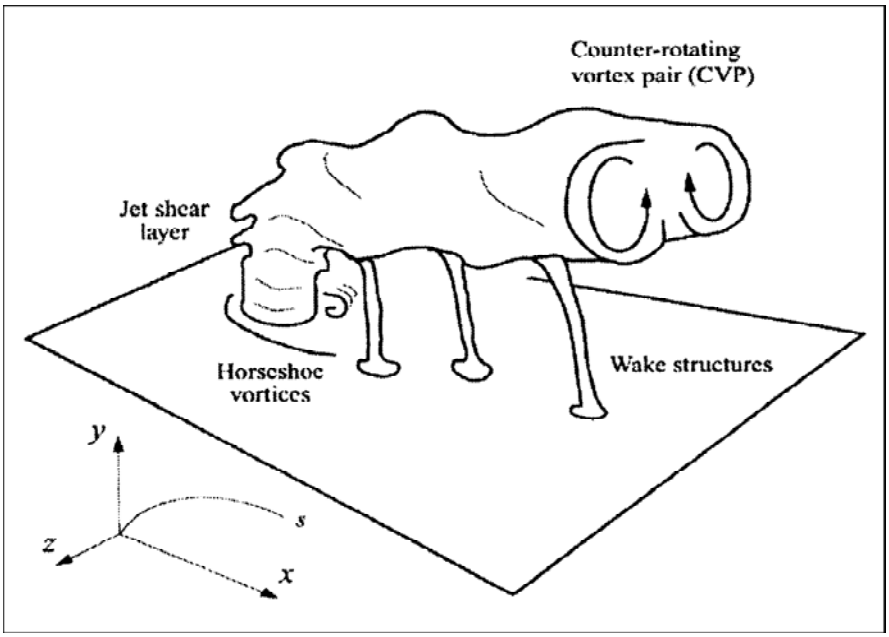

Figure 2.2: Vortical structures in a tee-junction as described by Meng and Pan (2001).

The physical characteristics of the injection jet were also examined by Meng and Pan (2001). A similarity solution for the jet centerline decay was validated for the downstream region. The rate at which the jet centerline decays is important since it describes the mixing in the flow. Finally as the jet travels downstream, it was shown to expand into the main flow while the centerline concentration decreases. Eventually the jet will expand to the point where the jet is no longer distinguishable from the main flow leading to a well-mixed status. Visualizations showed that as the jet is lifted in an

upward motion due to the CVP, the jet expands spanwise. In addition to the flow structure, the concentration probability function across the mixing layer was examined and revealed that on the upstream side of the jet, mixing is controlled by large-scale turbulent structures, and on the downstream side, diffusion dominates. This shows that eddy viscosity CFD models are will be more accurate for predictions downstream than upstream.

The accuracy of CFD models for tee-mixers has also been researched. Forney and Monclova (1995) used the k-ε model to analyze tee mixing quality by calculating the second moment of a simulated inert tracer. Water was injected into a pipe at a right angle and steady, single phase flow was simulated for injection to main pipe diameter ratio of $0.026 < d/D < 0.36$ with velocity ratios from 2 to 10. Several simulations were conducted and showed that changing the number of sweeps or decreasing the grid size only changed the predicted second moment of concentration by less than 3%. Initial values of the turbulent kinetic energy and the dissipation rate also had little effect on the results. Turbulent kinetic energy was found to be symmetrically distributed across the diameter of the pipe while concentration was found to be asymmetric with the largest concentration along the bottom of the pipe opposite the injection point. The simulated second moment of the tracer downstream from the tee junction was found to agree well with previously found experimental data showing that the k-ε model is a valid model for simulating tee-mixers.

The k-ε model was also used and validated for non-cylindrical geometries. Bertrand (1993) used the k-ε model to simulate tee-mixing in a square duct. A tracer was injected at a right angle into the main turbulent flow with a Reynolds number of 27,300

in the square duct. The geometry of the simulation used a jet-to-duct diameter ratio of 0.2 with a velocity ratio of 1 and 5. These velocity ratios led to the two distinctive conditions of a non-impinging and impinging jet. A velocity ratio of 5 caused the injection jet to impinge against the opposite wall. This simulation showed mixing to be poorer for the impinging condition and predicted a higher concentration of the injection fluid near the opposite wall. For the non-impinging condition, the highest concentration of the tracer was found on the symmetry plane of the duct with little mixing on the lateral side.

Sharma and Khokhar (2001) used the CFD program FLUENT to simulate tee mixers with both the k-ε model and the Reynold's Stress Model. Mixing was measured by calculating the temperature field. The temperature of the injection fluid was set at a higher temperature than the main pipe fluid, and 95% mixing was assumed to have been achieved when the bulk fluid temperature was within 5% of the main pipe's fluid's initial temperature. Velocity ratios of 17.1, 9.66, and 6.22 required 9, 11, and 13 pipe diameters, respectively, for 95% mixing. As expected, the simulations showed that the mixing length is a function of the velocity ratio. Both the RSM and k-ε model predicted the same pipe length required for 95% mixing but produce differing predictions for the highly turbulent region in the vicinity of the jet impingement. Experimental temperature data was shown to agree well with the simulations, especially for regions downstream near the 95% mixing point.

There has been a variety of dilution injection systems designed for paper machine head boxes. Voith and Metso are companies that produce two dilution systems that are currently used in the industry today. Invented by Begemann (1994) and associates, Voith patented a mixing system for mixing two liquids at the inlet of head box that is shown in

Figure 2.3. The system is designed so that CD (cross direction) basis weight and fiber orientation are influenced independently and locally. The system uses one main flow line and a secondary injection line with an adjustable angle and assumes there will be flow resistance downstream caused by the head box. The injection angle can range from 0 to 90 degrees. The input to the mixer is controlled by a single valve in the injection line. No valve is present in the input to the main flow line. The mixture volume flow rate is kept constant and independent of the velocity ratio. This is achieved by adjusting the injection angle and mixing angle in such a way that the decrease in the mixture volume flow rate caused by turbulence at the mixing point is exactly balanced by the Venturi effect, which by itself increases the mixture flow rate. The system also assumes constant pressure at the input and outputs of the mixer, but this is normal for a paper machine where pressure fluctuations can cause changes in the paper properties. An advantage of this system is that it does not require linearity in the control of the valves and actuators. Also the lack of an actuator in the main flow, which has a higher consistency and therefore greater percentage of fibers, prevents the problem of fiber wads forming.

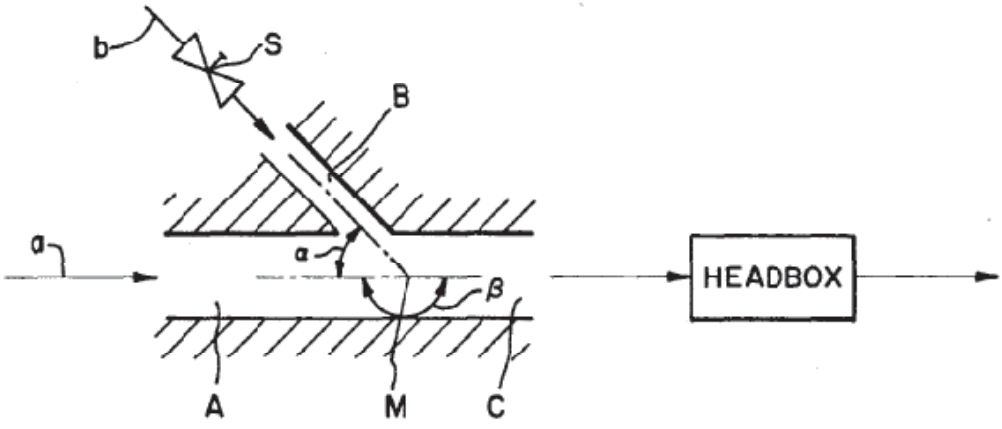

Figure 2.3: Schematics of the CD dilution system used by Voith.

Metso currently uses a dilution system patented by Jarmo Kirvesmaki (2009) and company. Older dilution systems have proven to be expensive because of the need for multiple valves, costly machining, and complex cleaning. This system attempted to solve these issues. This dilution system delivers all of the dilution flow through a single valve which is then fed into multiple mixing chambers. The dilution flow and the stock meet in the mixing chamber before being carried off through other ducts to the rest of the head box. There are multiple mixing chambers located across the width of the head box so that dilution flow can be injected at multiple desired locations. The ducts that carry the dilution flow open into the top part of the mixing chambers, but these ducts do not extend into the mixing chamber. Mixing takes place in the gap between the inlet ducts and the outlet. Outside of the mixing point, the mixing chamber is filled with dilution water. The pressure of the dilution water is higher than that of the stock flow, and the dilution water flows downward into the mixing chamber.

Research Gaps

Past research on tee mixers has not placed limits on the outlet flow rate, and most research used velocity ratios of 2 or greater. Many studies used velocity ratios that either centered the jet in the main flow or caused impingement on the opposite wall. Velocity ratios below 1 have historically been ignored. Furthermore the research on tee mixers has primarily focused on simple geometries like smooth pipes with no contractions or other complex structures. It is usually assumed that the injection pipe is centered along the main pipe at 90 degree angle. Most studies on tee-mixers have focused on chemical

mixers and not paper machine dilution systems. Paper dilution systems would differ from other studies since the water is not only at a higher temperature, but also contains solid wood pulp. The paper machine also creates upstream and downstream pressure resistances which are not commonly simulated. Also comparisons of simulated mixing using RSM and the k-e model are very limited. The k-ε model has been implemented for many CFD simulations of tee-mixers, but RSM is rarely used due to high computational costs.

CHAPTER 3

METHODS

The mesh for the T-junction for case 1 was created with Ansys Gambit with a mesh element size of 3 mm. Cases 2-4 required a more detailed mesh for analysis so an element size of 2.25 mm was used for these cases. Using the CFD program Fluent, water flowing through the tee-junction was simulated with a steady, two equation k-epsilon method. In order to compare the accuracy of turbulence models, the Reynolds stress method was also used for cases 2, 3, and 4. The density and viscosity of water were derived at a temperature of 120 F in order to approximate the actual temperature of pulp in a paper machine. Momentum, turbulent kinetic energy, and turbulent dissipation rate were all discretized with second order methods. As described in the Fluent manual, an implicit pressure based solver is used for incompressible flow. The SIMPLE algorithm described by Chorin (1968) was chosen to describe the relationship between the pressure and velocity. The SIMPLE algorithm relates velocity and pressure correction to solve for continuity and the pressure field. The full SIMPLE algorithm can be found in the Fluent manual (2006) or in a standard CFD textbook. To ensure convergence, residuals in the conservation equations were required to be below 10^{-4}.

The following boundary conditions were prescribed: total and initial gauge pressure at the main inlet, velocity at the injection inlet, atmospheric gauge pressure at the outlet, and no-slip on all the walls. These conditions are summarized in Table 3.1. The velocity condition at the injection inlet was derived from the velocity ratio, r. r is the ratio of the injection velocity to the desired outlet velocity that would produce the

required flow rate of 13 liters per second (lps). Based on the diameter of the main pipe, the needed outlet velocity was calculated to be 4.598 m/s. Therefore the injection velocity was calculated as r × 4.598 m/s. Five different velocity ratios were investigated: 0.25, 0.75, 1.33, 1.5, and 2.25. These ratios were chosen since according to previous research, they would not cause the jet to impinge on the opposite pipe wall. Cases 3 and 4 used the same model, boundary conditions, and velocity ratios as cases 1 and 2. The geometry of the mesh for cases 3 and 4 has been modified though so that a contraction is located in the main pipe near the injection point

Table 3.1: Boundary conditions used in simulations.

Location	Condition
Main Inlet	total and initial pressure (gauge)
Injection Inlet	velocity = r × 4.598 m/s
Outlet	static pressure =0 kPa (gauge)
Walls	no slip

In order to simulate realistic conditions in the head box of a paper machine, the simulations were designed to create an outlet flow rate of 13 liters per second (lps). Therefore the initial inlet (gauge) pressure was chosen so that in the case of zero injection, this inlet pressure would lead to the desired 13 lps at the outlet. The boundary conditions used to determine the necessary inlet pressure are shown in Figure 3.1. In Figure 3.1, q is a volumetric flow rate, *p* is the pressure, and *u* is the fluid velocity. The pressure at the main inlet was determined by first prescribing a pre-determined velocity corresponding to the 13 lps at the main inlet and zero flow at the injection inlet. The inlet velocity was determined from the cross-sectional area of the tee-junction and the desired

outlet flow rate of 13 lps. Simulations were then conducted using the following steps with reference to Figure 3.1.

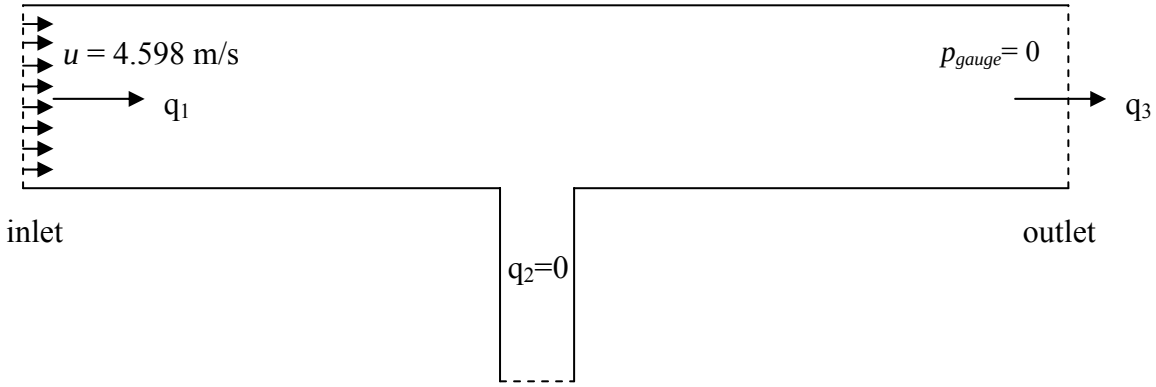

Figure 3.1: Boundary conditions used to determine the required inlet pressure

First a constant velocity profile with a magnitude of *u* was specified at the inlet using the determined velocity based on 13 lps. Fluent then calculates mass flow rate based on a velocity profile of a fluid entering a cell adjacent to the inlet from the following equation,

$$\dot{m} = \int \rho \vec{u} \cdot dA_c$$

where $\dot{m}$ is the mass flow rate, $\vec{u}$ is the specified fluid velocity vector at the inlet, and A_c is the area of each cell. The velocity at the injection inlet was set to zero so that $q_2 = 0$ as shown in Figure 3.1. A pressure outlet condition with a zero static pressure was specified

at the tee-mixer outlet. Here the inlet flow rate will equal the outlet flow rate, or $q_1 = q_3$. Using these results, the total and static pressure are measured at each node on the main inlet and averaged using the following equation where p is the pressure at each cell and $\overline{p}$ is the average pressure,

$$\overline{p} = \frac{1}{A_c}\int \rho \cdot d\,A_c$$

Next to perform the desired simulations, a pressure inlet was now specified at the main inlet as shown in Figure 3.2. Using the average pressures found for the zero injection case, the total and initial static pressures were prescribed at the inlet. Pressures are gauge and are relative to the atmospheric conditions. From these pressures, the initial fluid velocity magnitude at the inlet is then calculated using Bernoulli's equation as shown below,

$$p_0 = p_s + \frac{1}{2}\rho u^2$$

where p_0 is the total pressure, p_s is the static pressure, and u is the velocity magnitude. From this velocity magnitude and known flow direction, the initial velocity components and mass flow rate and volumetric flow rate are determined. The static pressure at the inlet is used to initialize the flow and the velocity magnitude, calculated through Bernoulli's equation, is an initial approximation for the inlet flow. Because this is a pressure driven flow, the actual fluid velocity will be lower based on downstream resistance.

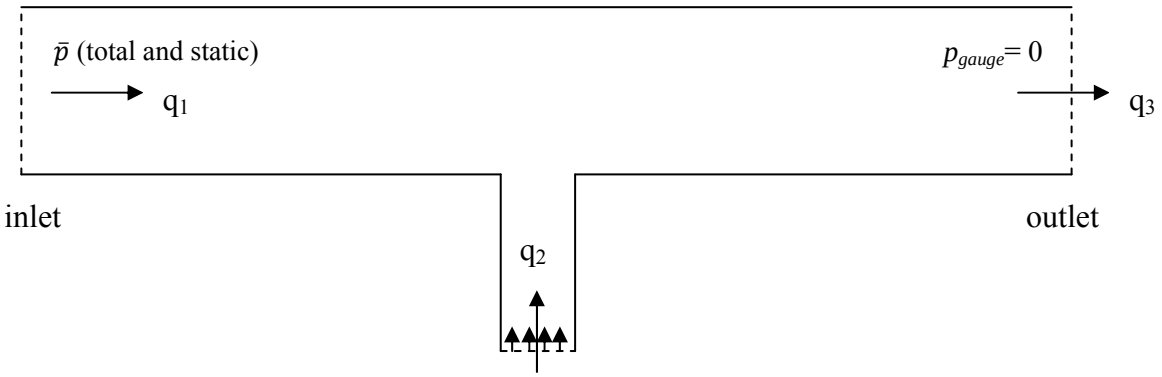

Figure 3.2: Boundary conditions used for all simulations

At the injection inlet, a velocity inlet boundary condition is chosen with a constant velocity profile based on the chosen velocity ratio. The volumetric outlet flow rate q_3 is then the sum of the two inlet flow rates, or $q_1 + q_2 = q_3$. .q_1 is initially an unknown quantity since it is dependent on q_2 and downstream resistances. At the outlet, a pressure outlet boundary condition with zero gauge static pressure was used again.

In a paper machine, flow through the head box is pressure driven, and the simulations were made to approximate such conditions. Therefore a pressure boundary condition is used at the inlet for all simulations. Flow rate cannot be specified at the outlet with a pressure condition at the inlet since this can lead to continuity problems. Therefore zero (gauge) static pressure was specified at the outlet. The zero static pressure is also used because this simulates real paper machine conditions, where the pulp will exit the head box as a free jet. Table 3.2 shows the inlet pressures used for cases 1-4. A flow rate of 13 lps for zero injection was achieved with each of these pressures. Cases 1-2 used the same inlet pressure, but since cases 3 and 4 had an added contraction, a greater inlet pressure was required.

Table 3.2: Inlet pressures (kPa) required for each case.

case	Inlet Pres.
1	192.4
2	192.4
3	210.0
4	210.0

Turbulent conditions were set at each boundary by specifying the turbulence intensity and hydraulic diameter. The hydraulic diameter, D_H, is the diameter of the respective pipe depending on the location of the boundary. The turbulence intensity, *I*, is determined from the following empirical equation described by the Fluent manual (2006),

$$I = \frac{u'}{u_{avg}} = 0.16\left(Re_{D_H}\right)^{(-1)/8}$$

where u_{avg} is the mean velocity and *u'* is the velocity fluctuations. The turbulence intensities used at the injection point are shown in Table 3.3. At the main inlet and outlet, turbulence intensity was specified by assuming the fluid velocity was the required 4.598 m/s with zero injection. This yielded a turbulence intensity of 3.1%.

Table 3.3: Turbulent intensity at the injection boundary as a function of r.

r	I (%)
0.25	4.35
0.75	3.80
1.33	3.53
1.5	3.48
2.25	3.31

In order to qualitatively model and visualize the mixing, passive particles were injected into the main water flow using the discrete phase model. First the domain of the main flow, water, was solved using the k-ε method. To solve this continuous domain, water was assumed to flow from both the main and injection inlets. After the main domain had converged, the passive particles were released from the injection inlet in order to visualize the flow coming from this section. The injected particles were set to use a random walk turbulent dispersion model in order to include the effect of turbulent velocity fluctuations.

When tracking particles in Fluent, the momentum of the fixed, continuous flow field and the injected particles can be either coupled or uncoupled. For the visualizations, an uncoupled model was used so that the injected particles did not exchange momentum or mass with the main flow. In this way, the injected particles did not affect the results of the solved continuous domain, but instead functioned as a means of post-processing and provided a visualization of the results. The validity of the choice of an uncoupled solution is based on the mass and momentum loading of the injected particles when compared to that of the main flow. Since the mass flow rate of the injected particles will be an order of magnitude smaller than those flowing from the main inlet, the injected particles will not noticeably impact the continuous phase.

As well as a visual critique of the mixing, a quantitative evaluation of the mixing was performed by measuring the concentration of the injected particles. To determine the concentration, a coupled solution had to be used so that the water and injected particles interacted. With a coupled solution, the injected particles and main flow now exchange momentum and mass. This required that the water's flow field and the injected particles'

flow fields be solved simultaneously. Using this solution, the concentration of the injected particles was measured at multiple points throughout the pipe.

Fluent Methods

Continuity and Momentum

$$\frac{\partial \rho}{\partial t} + \frac{\partial}{\partial x}(\rho u_x) + \frac{\partial}{\partial y}(\rho u_y) + \frac{\partial}{\partial z}(\rho u_z) = 0$$

The CFD program Fluent iteratively solves the conservation equations for continuity and momentum for all flows. Continuity is expressed in the above equation, and momentum is shown in the following set of equations. As the fluid being modeled is water, the flow is assumed to be incompressible. Both continuity and the resultant velocities from the momentum equations are used as criteria for convergence. Residuals are measured from the conservation equations and once they are below 10^{-4}, the simulations are assumed to be converged.

$$\mathbf{x:}\ \rho\left(\frac{\partial u_x}{\partial t} + u_x\frac{\partial u_x}{\partial x} + u_y\frac{\partial u_x}{\partial y} + u_z\frac{\partial u_x}{\partial z}\right) = \mu\left(\frac{\partial^2 u_x}{\partial x^2} + \frac{\partial^2 u_x}{\partial y^2} + \frac{\partial^2 u_x}{\partial z^2}\right) - \frac{\partial p}{\partial x} + \rho g_x$$

$$\mathbf{y:}\ \rho\left(\frac{\partial u_y}{\partial t} + u_x\frac{\partial u_y}{\partial x} + u_y\frac{\partial u_y}{\partial y} + u_z\frac{\partial u_y}{\partial z}\right) = \mu\left(\frac{\partial^2 u_y}{\partial x^2} + \frac{\partial^2 u_y}{\partial y^2} + \frac{\partial^2 u_y}{\partial z^2}\right) - \frac{\partial p}{\partial y} + \rho g_y$$

$$\mathbf{Z:}\ \rho\left(\frac{\partial u_z}{\partial t} + u_x\frac{\partial u_z}{\partial x} + u_y\frac{\partial u_z}{\partial y} + u_z\frac{\partial u_z}{\partial z}\right) = \mu\left(\frac{\partial^2 u_z}{\partial x^2} + \frac{\partial^2 u_z}{\partial y^2} + \frac{\partial^2 u_z}{\partial z^2}\right) - \frac{\partial p}{\partial z} + \rho g_z$$

k-epsilon turbulent method

In order to model turbulence, two models were used in Fluent. The first was the standard two equation k-ε method proposed by Launder and Spalding (1972). The momentum and continuity equations are first time averaged. Then, based on the kinetic theory of gases, the turbulent viscosity is assumed to be a function of the turbulent kinetic energy, k, and the viscous dissipation rate, ϵ. By assuming k and ϵ to be transported properties and solving the relevant equations for them, the velocity field can be determined. The standard k-ε model found in textbooks like Turbulent Flows by Pope (2000) was used for all simulations. This model intrinsically requires an important assumption, known as the Turbulent Viscosity hypothesis, which states that the Reynold's stress tensor is proportional to the mean strain rate. As stated in Turbulent Flows (2000), the consequence of this assumption is that the accuracy of the model will vary with the geometry and conditions of the flow. Furthermore since the Reynold's stresses are the mechanism through which the turbulent fluctuations impact the mean flow, a relationship between the mean straining and Reynold's stresses describes how the geometry and flow conditions affect the turbulence. For simple shear flows and geometries like pipe flow, Pope states this assumption has proven to be very reasonable. However with more complex geometries like a contraction, the assumption that there is a relationship between the local strain rate and the stress is not valid, and therefore the k- ϵ model will be less accurate. Pope states that experiments have shown that the effects of sudden geometry changes like contractions propagate much farther downstream than expected that so that local effects no longer completely determine strain rate. Because of

this, the Reynold's stress model is used for the simulations with contractions since it does not rely on the turbulent viscosity hypothesis and the concept of eddy diffusivity.

Reynold's Stress Method (RSM)

The general Reynolds stress method equations as described in textbooks like Turbulent Flows by Pope (2000) was used for the simulations. The Reynolds stress methods model transport equations for the Reynolds stresses and solves them numerically with an equation for dissipation and other conservation equations. The Reynolds Stresses are the physical mechanisms through which the turbulent velocity fluctuations impact the mean flow. The RSM method requires seven equations to be solved. An important distinction is that RSM does not rely on the turbulent viscosity hypothesis and local isotropy. This causes RSM to be more accurate than the k- ϵ model, but the RSM is more computationally expensive since it must solve seven equations. Furthermore, unlike the k-ε model, the RSM can handle rapid changes in strain rate allowing it to more accurately model complex situations like swirling flows and contractions.

Discrete Phase Model (DPM)

The discrete phase model is used to simulate the flow of injected particles. The typical solver used to evaluate fluid flow implements an Eulerian solution where the fluid phase is treated as a continuous phase by solving the Navier Stokes and continuity equations. The discrete phase model creates a second phase, consisting of spherical particles, in a Lagrangian frame of reference dispersed in the continuous main phase. In the continuous phase, the fluid is assumed to have infinitesimally small particles;

however, the discrete phase uses particles of a given diameter and solves for momentum and continuity on each particle. There are two ways in which these phases can interact: uncoupled and coupled. In an uncoupled solution, the fluid phase imparts momentum on each particle, but the injected particles do not enact forces on the continuous fluid and alter their results. Because of this, the fluid phase is solved first, and then particle trajectories can be calculated integrating the following force balance on each particle,

$$\frac{du_p}{dt} = F_D(u - u_p) + F_{pr} + F_x$$

In this equation, u is the fluid velocity, u_p is the particle velocity, F_D is the drag force per unit particle mass, F_{pr} is the force due to the pressure gradient in the fluid, and F_x is a set of additional forces dependent on the density gradient and other special circumstances. The pressure gradient force is described by the following equation,

$$F_{pr} = \left(\frac{\rho}{\rho_p}\right) u_{p_i} \frac{\partial u}{\partial x_i}$$

where ρ is the fluid density and ρ_p is the density of the particles. A detailed description on the drag force and other forces, F_x, can be found in the Fluent manual (2006).

This uncoupled solution was used for the mixing visualizations. The particles were chosen to have a density and viscosity equivalent to that of water with a particle diameter of 1 micron. The particles were given an initial velocity equivalent to the injection inlet boundary condition velocity used when solving the continuous phase and

were required to reflect off walls. The mass flow rate of the particles was based off this initial velocity, particle density, and cross sectional area of the injection pipe.

An uncoupled solution is valid when the mass flow rate of the injected particles is much lower than that of the continuous flow. To ensure the accuracy of the results, the injection flow rate should be no more than 10% of the main flow. Since the mass flow rate of the injected particles in these simulations were an order of magnitude smaller than those flowing from the main inlet, the injected particles did not noticeably impact the continuous phase. For the simulated geometry and flow conditions, an uncoupled solution provided an accurate method to model the paths of the injected particles.

In order to establish a quantitative measurement of the mixing in the tee-junction, a coupled discrete phase model was used in Fluent to measure the concentration of the injected particles throughout the pipe. The concentration of particles can only be calculated using a coupled approach. This coupled solution now assumed that the injected particles would impact the continuous flow field. When the two phases are coupled, the continuous phase and discrete phase will exchange momentum and mass. This coupling requires that flow in the two phases be solved simultaneously. Furthermore, the trajectories of the particles are predicted in Fluent by solving a force balance on each particle in the Lagrangian frame. The equations of motions of the particles were solved using a 5^{th} order Runge Kutta method.

The mixing was quantified by using the method described by Forney (1989) where the second moment of the concentration of a tracer is measured at various locations in the pipe. This is useful since the second moment describes the spread of the particle concentration, or more directly the diffusion of the injected particles across the

pipe diameter. Therefore as the second moment decreases, the concentration of the particles across the diameter of the pipe becomes more similar at each measured location. An even distribution of the particles represents quality mixing.

In the steady state simulations in Fluent, the discrete phase can be viewed as a stream of particles rather than large number of particles distributed throughout the domain. Furthermore the total mass of particle entering the domain is equal to the mass of particles leaving. Therefore the DPM concentration will be calculated based on the particle residence time in each cell. Fluent uses the following equation to calculate the mass concentration, c, of particles for steady state flows:

$$c = \frac{\dot{m} * t}{V_c}$$

where $\dot{m}$ is the mass flow rate of the particles, t is the residence time in each cell, and V_c is the volume of each cell. The second moment of concentration, M, is calculated based on the average concentration,$\bar{c}$, using the following equation with N as the number of cells and :

$$M = \sqrt{\frac{1}{N}\sum_{i=1}^{N}(c_i - \bar{c})^2}$$

CHAPTER 4

RESULTS AND DISCUSSION

Flow Rates

The following table and graphs show comparisons of the flow rates for cases 1-4. All of these results were obtained using the k-ε method for turbulent flows unless noted otherwise. Results were taken after convergence had been achieved with respect to mass conservation and momentum. Table 4.1 shows the outlet flow rates obtained from the k-ε and RSM simulations with all of the values normalized to the desired flow rate of 13 lps. Cases 1 and 2 were simulated for velocity ratios of 0.75 to 2.25. Because the mixing was already found to be poor at r = 0.75 for these cases, velocity ratios below 0.75 were not investigated since previous research had shown the injected particle diffusion across the pipe to be proportional to velocity ratio. With cases 3 and 4, acceptable mixing was achieved with a velocity ratio of 0.75. As a result, velocity ratios greater than 1.33 were not investigated since it was unnecessary. Velocity ratios below 0.25 though were not simulated since previous research has shown that such small ratios cause the injection jet to act as a wall source which produces poor particle dispersion.

Table 4.1: Outlet flow rates for each case as a function of velocity ratio, r.

r	case 1	case 2	case 2 (RSM)	case 3 (ke)	case 3 (RSM)	case 4 (ke)	case 4 (RSM)
0.25	NA	NA	NA	1.014	0.999	1.008	0.993
0.75	1.013	1.030	1.021	1.025	1.010	1.015	1.004
1.33	1.018	1.036	1.034	1.036	1.021	1.020	1.015
1.5	1.019	1.038	1.039	NA	NA	NA	NA
2.25	1.026	1.053	1.058	NA	NA	NA	NA

An acceptable outlet flow rate is 1.01 since this fulfils the requirement of a maximum flow rate change of 1% from the zero injection case. As shown in Table 4.1, all of the flow rates for cases 1 and 2, the non-contraction geometries, were greater than 1.01 with case 2 generating the highest flow rates. The most interesting aspect of Table 4.1 though is the results of the contraction geometries, cases 3 and 4. The lower flow rates of the contraction cases are expected since they contain sources of resistance which dissipate the increased energy from the injection flow. The results for both cases k-ε and RSM simulations show there is potential to find outlet flow rate below 1.01. With the contraction located either before or after the injection, velocity ratios of 0.25 and 0.75 produced flow rates below 1.01. In fact the k-ε and RSM results for case 4 show flow rates that are lower than the other cases.

When comparing the results of the two turbulent models for each individual case, it can be seen in Table 4.1 that the RSM results are only at most 2% smaller than those of the respective k-ε model. This shows that the two turbulence models produce similar results. As explained in Turbulent Flows by Pope (2000), the RSM has been shown to perform with increased accuracy over the standard k-ε model for axisymmetric contractions like those found in cases 3 and 4. This would then indicate that the lower flow rates found for the contraction cases using the Reynold's stress method are more accurate than those produced with the k-ε model. With a paper machine, a 1% change in flow rate is significant, so the 2% difference in the turbulent model results is a significant outcome and warrants the RSM being chosen as the preferred model. However convergence for the RSM required over 5 times as many iterations as the k-ε model and an order of magnitude more time.

Finally, the lower flow rates for case 4 shown in Table 4.1 indicate that placing the contraction after the injection leads to the lowest flow rates. This is expected as the contractions can be viewed as sources of flow resistance in the main pipe. Since the fluid is pressure driven, contractions that reduce the fluid pressure will lower the fluid flow rate. A contraction after the injection will directly reduce the added energy caused by the injection since it acts as a source of viscous dissipation. In the limiting case of very high downstream resistance, the effects of the injected flow would be mitigated due to the high resistance, and instead, the outlet flow rate would be controlled by the inlet flow rate due to the constant pressure condition. When the contraction is located before the injection, the reduction in energy caused by the contraction will not affect the injection flow. This leads to higher flow rates for case 3 when compared to case 4.

Figure 4.1 shows the outlet flow rates found for cases 1-4 as a function of velocity ratio. Figure 4.1 demonstrates that flow rate tends to increase with velocity ratio linearly. Outlet flow rates are lowest for cases 3 and 4, the contraction cases, and highest for case 2, the geometry where the injection pipe was not centered. Because the non-centered injection pipe produced the highest flow rates, a centered pipe was used for both of the contraction cases. It can be concluded that with further investigation, a velocity ratio producing an acceptable flow rate for case 1 could potentially be found. However because of the poor mixing found in case 1 as shown in the mixing results, simulations using the standard tee-junction of case 1 for velocity ratios below 0.75 were not conducted.

The key lines to examine in Figure 4.1 are those for cases 3 and 4. These are the only cases whose flow rates are below the 1.01 mark. The k-ε results for case 4 show that

a velocity ratio of 0.25 to 0.75 does not alter the flow rate by more than 1%. The RSM results for both cases 3 and 4 also show that a velocity ratio of 0.75 and below will satisfy the flow rate condition. Unlike case 3 though, the case 4 RSM show that a velocity ratio of 1.0 would not noticeably impact the outlet flow rate. A contraction located after the injection allows for not only lower flow rates, but also a wider range of velocity ratios.

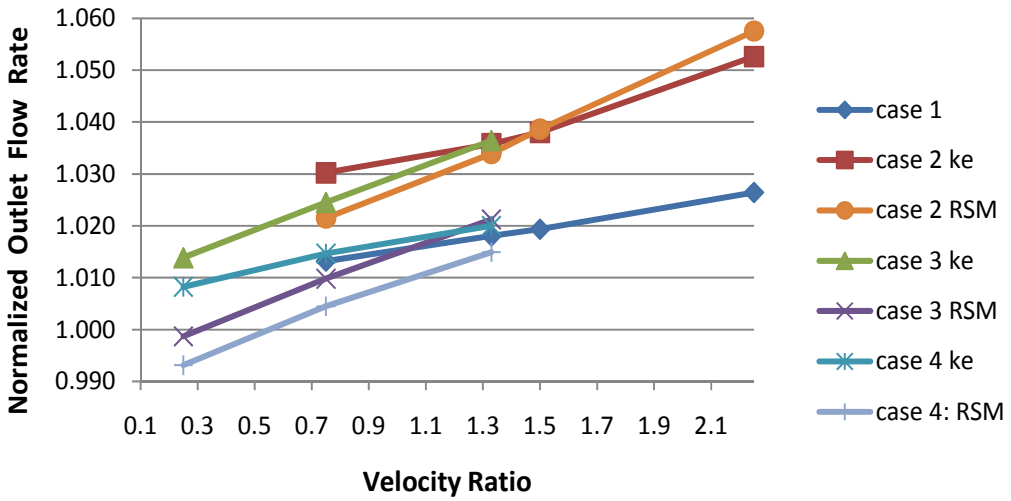

Figure 4.1: Outlet flow rates as a function of velocity ratio for each case

It is also worth noting that RSM simulations did not yield the same trend of results for case 2 as with cases 3 and 4. For cases 3 and 4, where a contraction was used with a centered injection pipe, the RSM results were lower than the k-ε flow rates at each velocity ratio. As seen in Figure 4.1 for case 2, at higher velocity ratio, the Reynold's stress model actually produces higher flow rates than the k-ε model. This is due to the differing geometries of cases 2 and 3 and the turbulent viscosity hypothesis. Furthermore the non-centered injection pipe location created a swirling flow that was not present any

of the other simulations. According to Turbulent Flows by Pope (2000), the Reynold's stress model is more suited to handle swirling flows where vorticity production has increased and local isotropy cannot be assumed. Vorticity was seen to increase with velocity ratio, and for these higher velocity ratios the Reynold's stress models predicted higher flow rates for case 2.

Mixing

Quantitative Analysis

In order to evaluate mixing, the second moment is measured at five different planes downstream from the injection points for the two contraction cases. The contraction cases were numerically evaluated since they showed the lowest flow rates. Mixing is then characterized by the size of the second moment of concentration. Table 4.2 shows the values of the second moment measurements for cases 3 and 4 as a function of distance and velocity ratio. The distance x is normalized to the pipe diameter D. Since the concentration is a function of flow rate, the second moment is normalized to the average concentration for each velocity ratio. A smaller second moment of concentration indicates that the distribution of the injected particles has become more equalized across the diameter of the pipe. Moreover, the smaller second moment shows that there is not a high concentration of particles in one location of the pipe. Therefore a lower second moment is equivalent to the desired high quality mixing. As shown in Table 4.2, the second moment decreases as the distance downstream increases. Furthermore it can also be seen that the second moment decreases with velocity ratio. This shows that the

injected particles spread across the diameter of the pipe as they move downstream from the injection which proves that increased velocity ratios leads to more effective mixing.

Table 4.2: Second moment of concentration as a function of distance

	r = 0.25		r = 0.75		r = 1.33	
x/D	case 3	case 4	case 3	case 4	case 3	case 4
5.0	1.75	2.12	1.50	1.87	1.54	1.98
5.8	1.55	2.13	1.41	1.84	1.35	1.81
6.7	1.49	2.04	1.34	1.87	1.29	1.60
7.5	1.45	1.90	1.29	1.74	1.27	1.50
8.3	1.46	1.80	1.33	1.68	1.26	1.58

Figure 4.2 graphically shows the second moment of concentration for cases 3 and 4 as a function of downstream distance. When comparing cases 3 and 4, Figure 4.2 shows that all of case 3's second moments of concentrations are lower than those of case 4. This shows that placing a contraction before the injection leads to greater particle dispersion than when the contraction is placed after the injection. When comparing the actual values between the two cases using Table 4.2, case 4 on average only produces about 20% higher second moments of concentration. Within each individual case, the graph further supports the conclusion that increased velocity ratio leads to lower second moments and therefore more effective mixing.

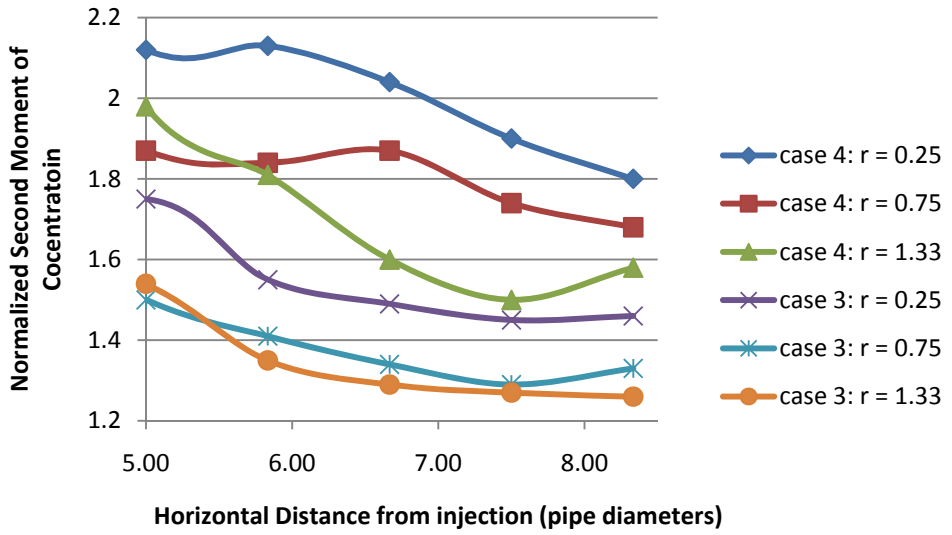

Figure 4.2: Second moments of concentration as a function of distance for cases 3 and 4

Visualizations

Figures 4.3-4.6 show the mixing for cases 1-4 for a velocity ratio of 0.75. Flow is from the right to the left. The blue lines represent the main flow. The red lines represent the trajectories of the injected particles. The particles, the red lines, do not interact with the continuous flow, the blue lines. The blue lines simply show the pathlines of the continuous flow and are shown only to demonstrate the geometry of the main pipe. As stated, a stochastic random walk model was used to simulate the effect of the turbulent velocity fluctuations. The key result to exam in Figures 4.3-4.6 is the distance required for the red lines, the injected particles, to spread completely across the diameter of the pipe. When the injected particles, red, reach the opposite wall of the pipe, the top blue line, the desired mixing has occurred. Figures 4.3-4.6 show the mixing near the injection point up to the first resistance orifice. The orifice is not actually a part of the dilution system, but instead it was only added to simulate downstream resistance in the head box.

This covers a range of 10 pipe diameters. As seen in Figures 4.3 and 4.4, the injected particles do not rapidly reach the opposite wall from the injection point. In fact in case 1, shown in Figure 4.3, the injected particles never enter the vicinity of the opposite wall before the resistance orifice. For the contraction cases, as shown in Figures 4.5 and 4.6, the injected particles spread completely across the pipe within 5 pipe diameters, or half the shown distance. This is especially true for case 3, where the contraction is located before the injection. Figures 4.5 and 4.6 show that cases 3 and 4, the contraction geometry, clearly create superior mixing to that of cases 1 and 2 since the injected particles reach the opposite pipe wall within 5 pipe diameters. Cases 1 and 2, Figures 4.3 and 4.4, have insufficient mixing. A more extensive set of visualizations for each case can be found in the Appendix. The Appendix shows the mixing for each case for a wide range of velocity ratios from 0.25 to as high as 2.25.

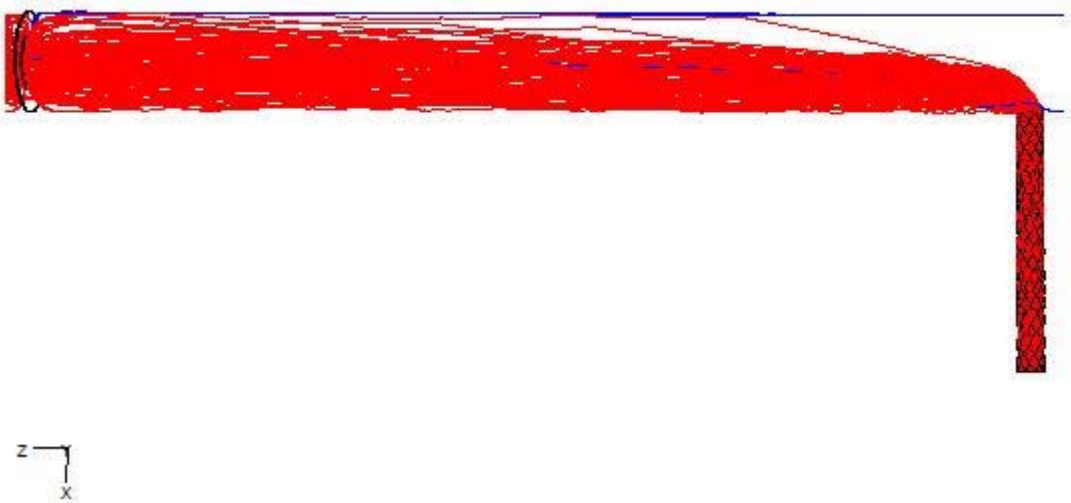

Figure 4.3: Case 1: Particle traces from injection to orifice; Red = injection particle, Blue = trace of pipe walls, r = 0.75, Re_main= 476,411. Re_inj = 99,676.

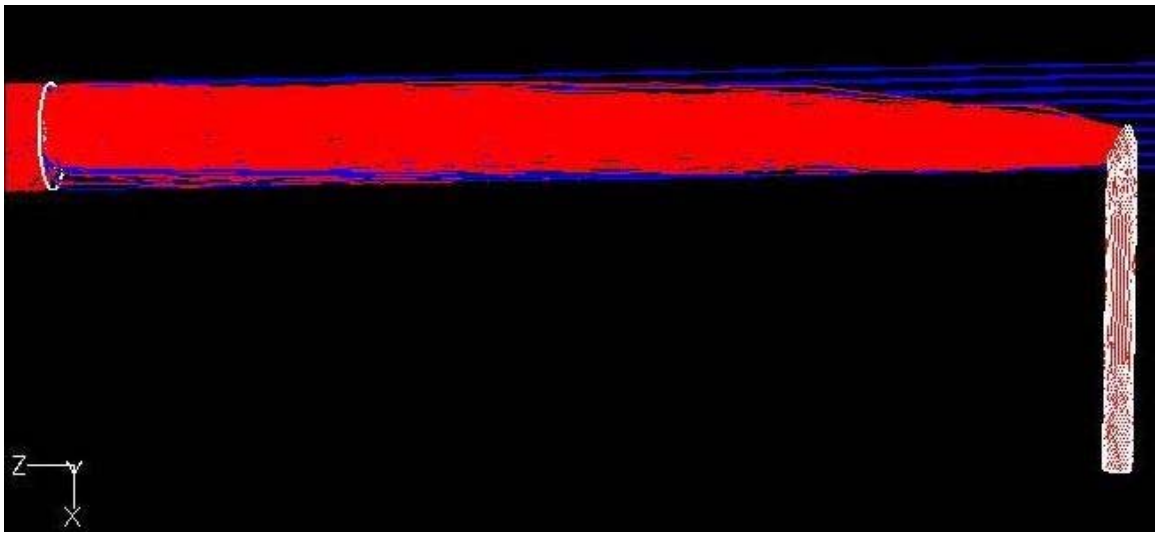

Figure 4.4: Case 2: Particle traces from injection to orifice; Red = injection particle, Blue = trace of pipe walls , r = 0.75, Re_main= 482,820. Re_inj = 99,676.

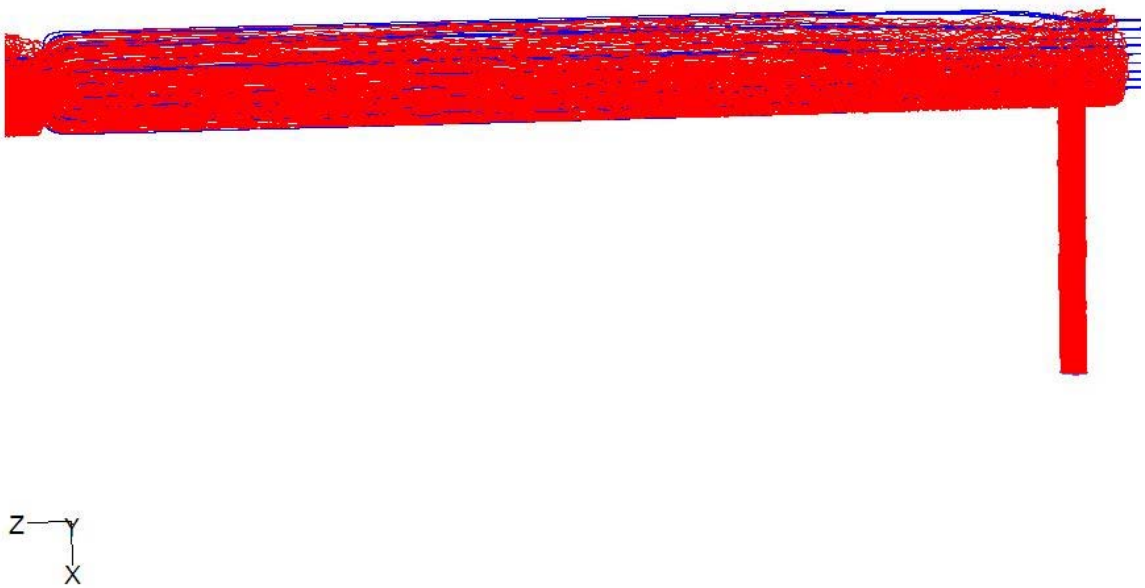

Figure 4.5: Case 3: Particle traces from injection to orifice; Red = injection particle, Blue = trace of pipe walls, r = 0.75, Re_main= 482,820. Re_inj = 99,676

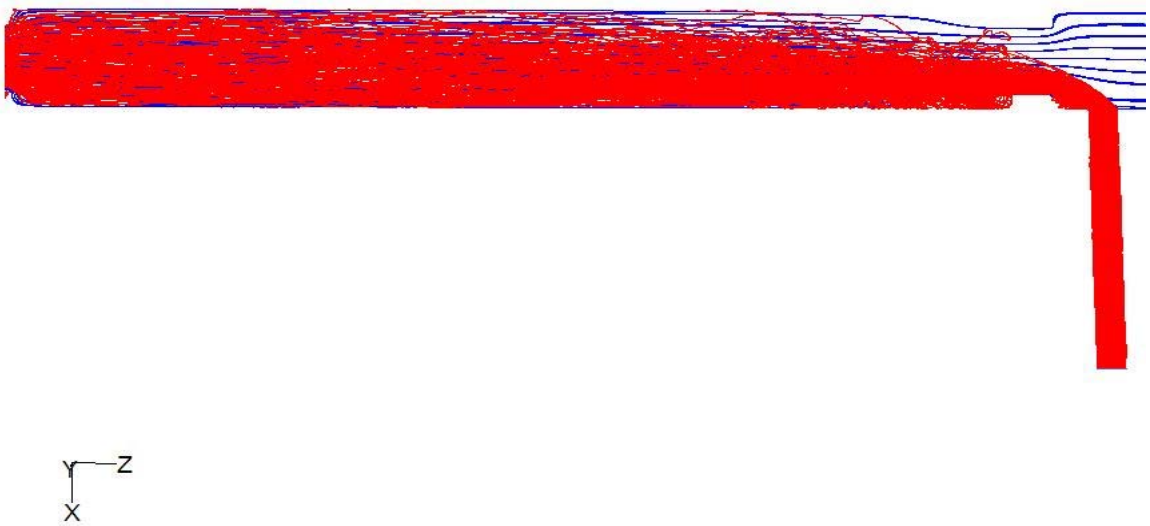

Figure 4.6: Case 4: Particle traces from injection to orifice; Red = injection particle, Blue = trace of pipe walls, r = 0.75, Re_main= 482,820. Re_inj = 99,676

Pressure

Table 4.3 shows the static pressure (gauge) for cases 3 and 4 as a function of velocity ratio and horizontal distance from the injection. The distance is shown in terms of pipe diameters from the injection point, and pressures are normalized in terms of the inlet pressure of 210 kPa. As can be seen in the Table 4.3, the static pressure for case 3 is very similar to that of case 4. Table 4.3 also shows that though the pressure increases with velocity ratio, it does not vary significantly.

Table 4.3: Static pressure for cases 3 and 4 as a function of velocity ratio and distance

	r = 0.25		r =0.75		r =1.33	
x/D	case 3	case 4	case 3	case 4	case 3	case 4
-1.7	0.7833	0.7897	0.7964	0.8049	0.8101	0.8226
3.3	0.6251	0.6074	0.6381	0.6137	0.6515	0.6206
15.0	0.0053	0.0011	0.0054	0.0010	0.0055	0.0009

Since the cross sectional area of the main pipe is 10 times greater than that of the injection pipe, the flow rate of water released from the main inlet was much greater the injection flow rate. Also the velocity ratios were chosen so that they would not noticeably change the flow rate. The consequence of this difference in flow rate and the constant fluid pressure at the inlet is that the injected fluid does not have a large effect on the bulk flow static pressure. This is demonstrated by Figure 4.7 which shows the static pressure throughout the main pipe for the contraction cases with a velocity ratio of 0.25. For a paper machine though, the small changes in flow rate caused by the small changes in pressure are significant. Near the injection, case 3 has a slightly higher static pressure than case 4 as seen in Figure 4.7.

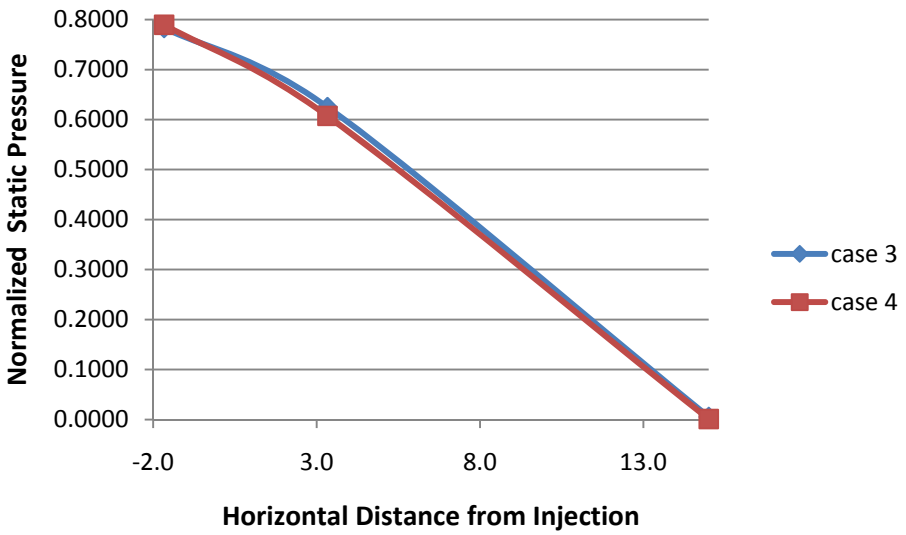

Figure 4.7: Static pressure measured throughout the pipe for r = 0.25

Another important quantity often measured in tee-mixers is pressure drop. Figure 4.8 shows the static pressure drop across the injection point for cases 3 and 4. The pressure drop is measured as the difference between the pressure at -1.7 and 3.3 pipe diameters from the injection point. For both cases 3 and 4, the pressure drop increases with increasing velocity ratio. The pressure drop for case 4 though, as shown in Figure 4.8, increases more rapidly with velocity ratio than case 3, which stays near 16%.

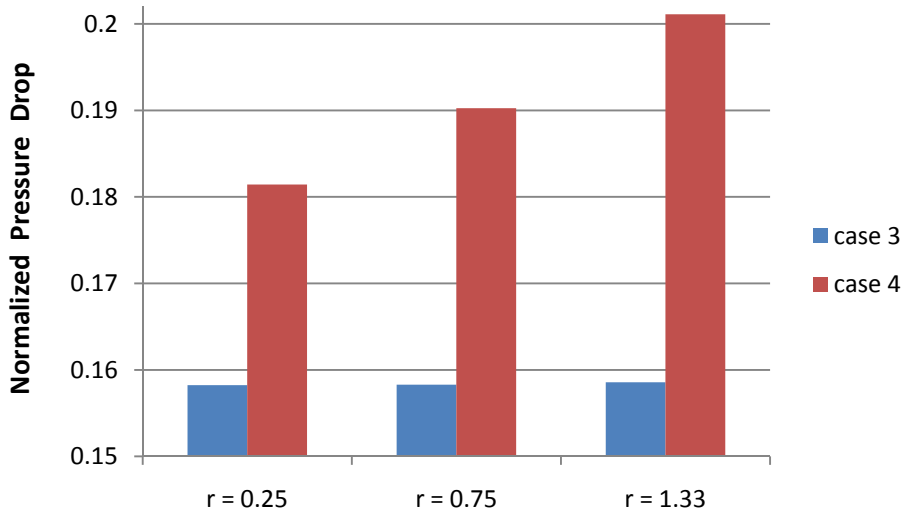

Figure 4.8: Pressure drop across the injection for cases 3 and 4.

The trends shown in Figure 4.8 can be explained through the location of the contractions. Through the conservation of energy, the pressure gradient in the pipe is balanced by the viscous effects of the pipe and more noticeably here, the contractions. Although the injected flow increases the energy in the combined flow, this increase in energy is reduced by the increase in viscous dissipation due to the contractions. This shows why the cases without contractions have higher flow rates. Since the flows are pressure driven, it is then expected that the contraction cases which have lower flow rates would then experience greater pressure losses. This is demonstrated in Figure 4.8 where pressure drops ranging from 16%-20% are shown. With case 4, the combined fluid flows through the contraction. This contraction then directly reduces the energy of the combined flow. With case 3, the contraction is located before the injection, so the combined flow will not be impacted by the contraction resistance. This explains why the case 4 pressure drops are greater than those of case 3 and also the reduced influence on the pressure drop of case 3.

CHAPTER 5

CLOSING

The goal of the project was to design a dilution system that will rapidly mix the dilution water with the main flow while at the same time not altering the outlet flow rate by more than 1%. All of the results indicate that placing a contraction after the injection, the geometry of case 4, is the most promising with quality mixing and lower flow rates. The tee-junctions without contractions showed poor mixing for lower velocity ratios, and for higher velocity ratios, the flow rates were too large. Furthermore a non-centered location of the injection pipe yielded the greatest increase in flow rates and did not noticeably improve the mixing compared to the results of a centered injection pipe. By measuring the second moment of concentration, it was shown that increasing the velocity ratio increased the dispersion of the injected particles. When comparing the effect on mixing of the contraction locations, a contraction before the injection, case 3, was shown to have about 20% lower second moments than a contraction after the injection, case 4, within 10 pipe diameters of the injection point. From the second moment data, it can be inferred that a contraction before the injection results in more rapid mixing than a contraction after the injection. Visually, both contraction cases showed acceptable mixing, but the outlet flow rates produced by case 3 were slightly higher than those of case 4. While case 3's flow rates were less than 2% higher than those of case 4, it is desirable to have as small of a flow rate change as possible. An acceptable flow rate change and rapid mixing for these contraction cases was found at a velocity ratio of 0.25-0.75 within the first 10 pipe diameters. Overall placing a contraction before the injection

led to better mixing, but when the contraction was located after the injection, the flow rates were lower. The change in flow rate is the most important factor for a paper machine, and since case 4 provided adequate mixing and the lowest flow rates, a contraction after the injection proved to be the best geometry.

The k-e method provided sufficient results for all simulations, the RSM predicted lower flow rates for the contraction cases at the cost of increased computational time. While the flow rates computed using the Reynold's stress methods were only at most 2% smaller than those of the k-ε model, increased accuracy is paramount for a paper machine where small changes in flow rate will noticeably alter the dimensions of the paper sheet. Since previous studies have documented by Pope (2000) in his textbook demonstrated that the Reynold's stress methods are more accurate than the k-ε model for contractions, the Reynold's stress model should be used to simulate dilution systems containing contractions.

The simulations also showed that the static pressure for case 3 and case 4 was very similar throughout the majority of the pipe. The pressure drop across the injection increased with velocity ratio for both contraction cases. When the contraction was located after the injection, pressure drops were calculated to be between 18% and 20%. Higher pressure drops were associated with higher velocity ratios. When the contraction was located before the injection, a pressure drop of around 16% was found. For this geometry the pressure drop only slightly increased with velocity ratio. A dilution system with a contraction after the injection point showed effective mixing with injected particles rapidly dispersed with a low flow rate change for a velocity ratio potentially as high as 1.0.

APPENDIX A

MIXING IMAGES

Case 1

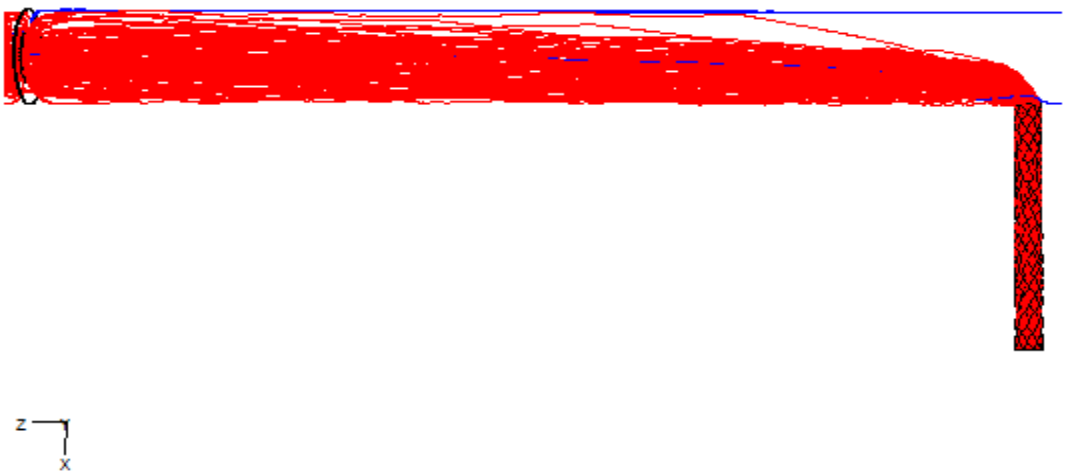

Figure A.1: Particle traces from injection to orifice; Red = injection particle, Blue = trace of pipe walls. r = 1.33, Re_main= 460,210. Re_inj = 176,756. P = 192.4 kPa.

Figure A.2: Particle traces near orifice; Red = injection particle, Blue = trace of pipe walls. r = 1.33, Re_main= 460,210. Re_inj = 176,756. P = 192.4 kPa.

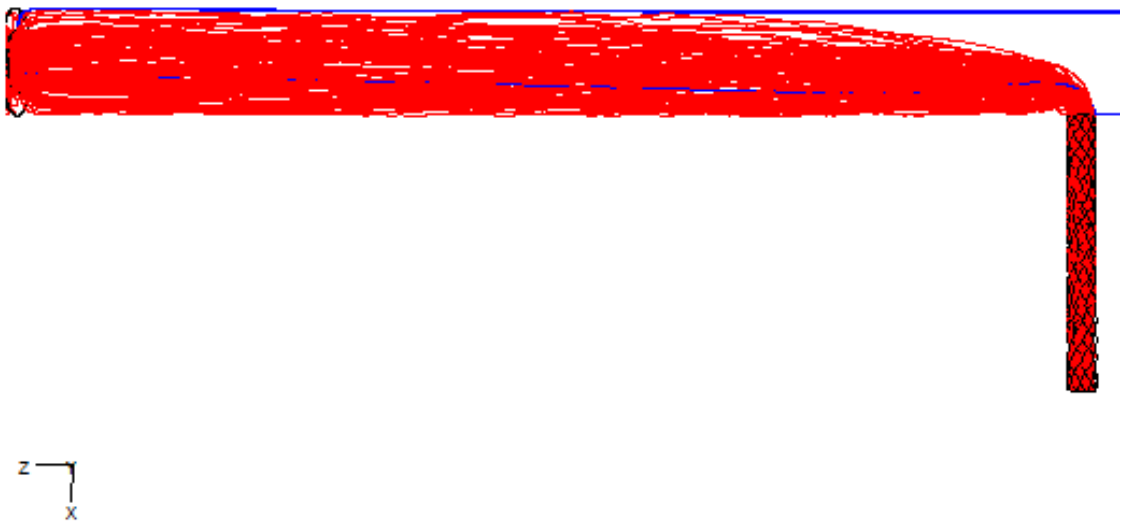

Figure A.3: Particle traces from injection to orifice; Red = injection particle, Blue = trace of pipe walls r = 1.50, Re_main= 455,400. Re_inj = 199,360. P = 192.4 kPa.

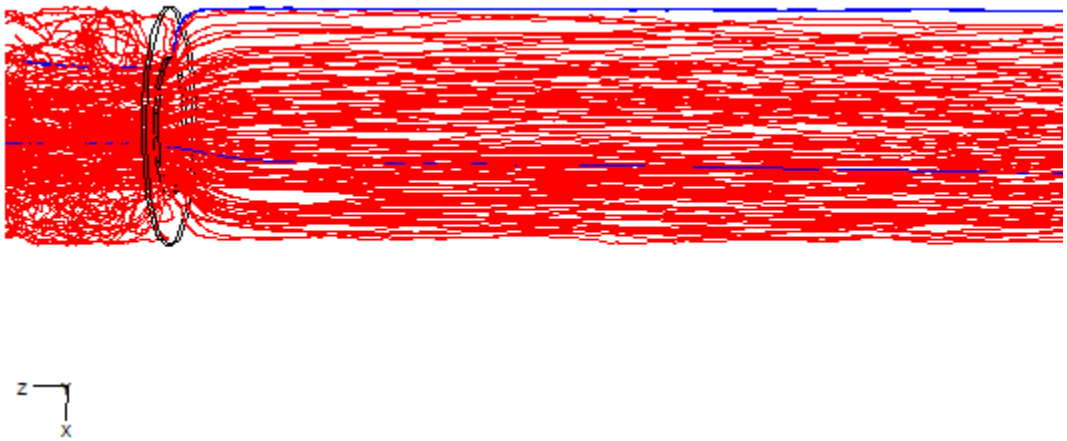

Figure A.4: Particle traces near orifice; Red = injection particle, Blue = trace of pipe walls. r = 1.50, Re_main= 455,400. Re_inj = 199,360. P = 192.4 kPa.

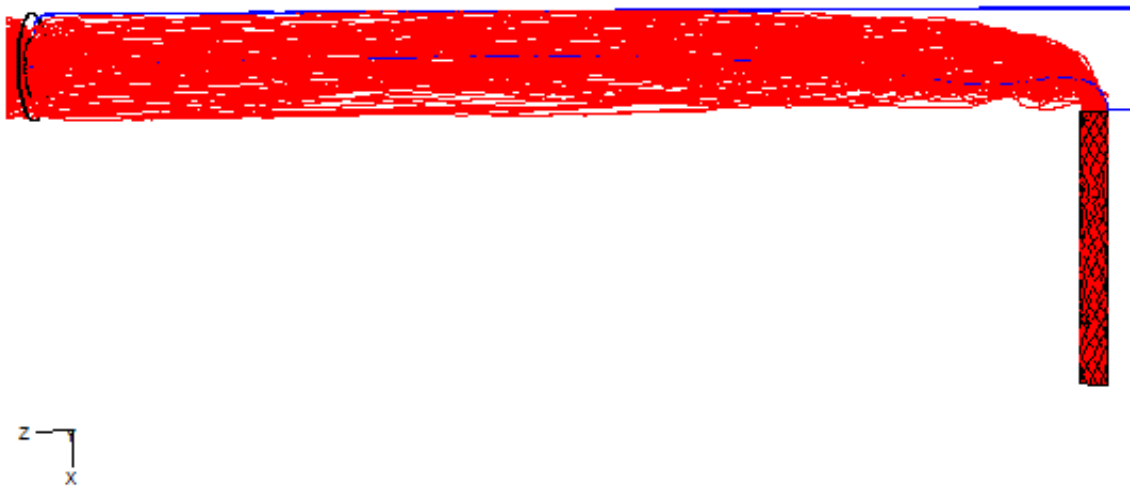

Figure A.5: Particle traces from injection to orifice; Red = injection particle, Blue = trace of pipe walls. r = 2.25, Re_main= 434,856. Re_inj = 299,054. P = 192.4 kPa.

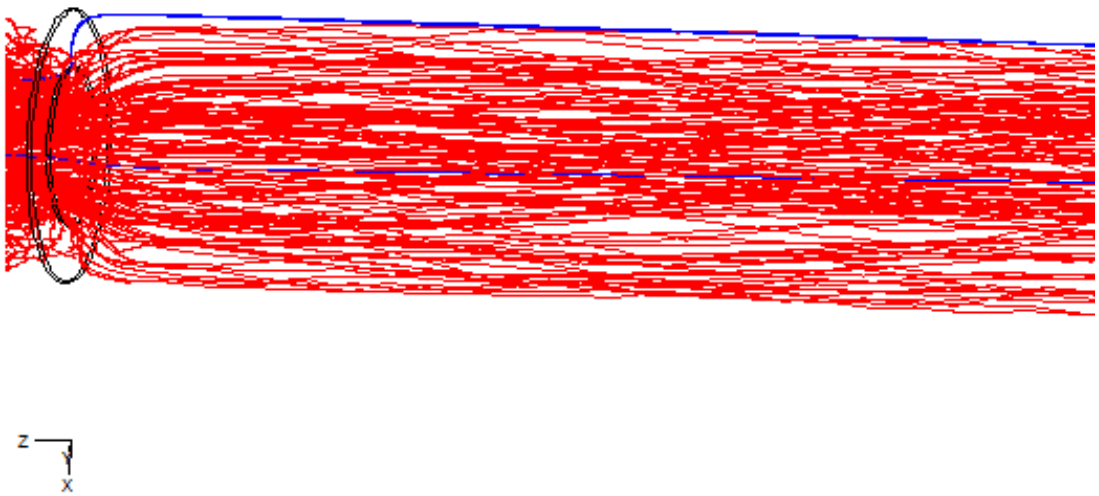

Figure A.6: Particle traces near orifice; Red = injection particle, Blue = trace of pipe walls. r = 2.25, Re_main= 434,856. Re_inj = 299,054. P = 192.4 kPa.

Case 2

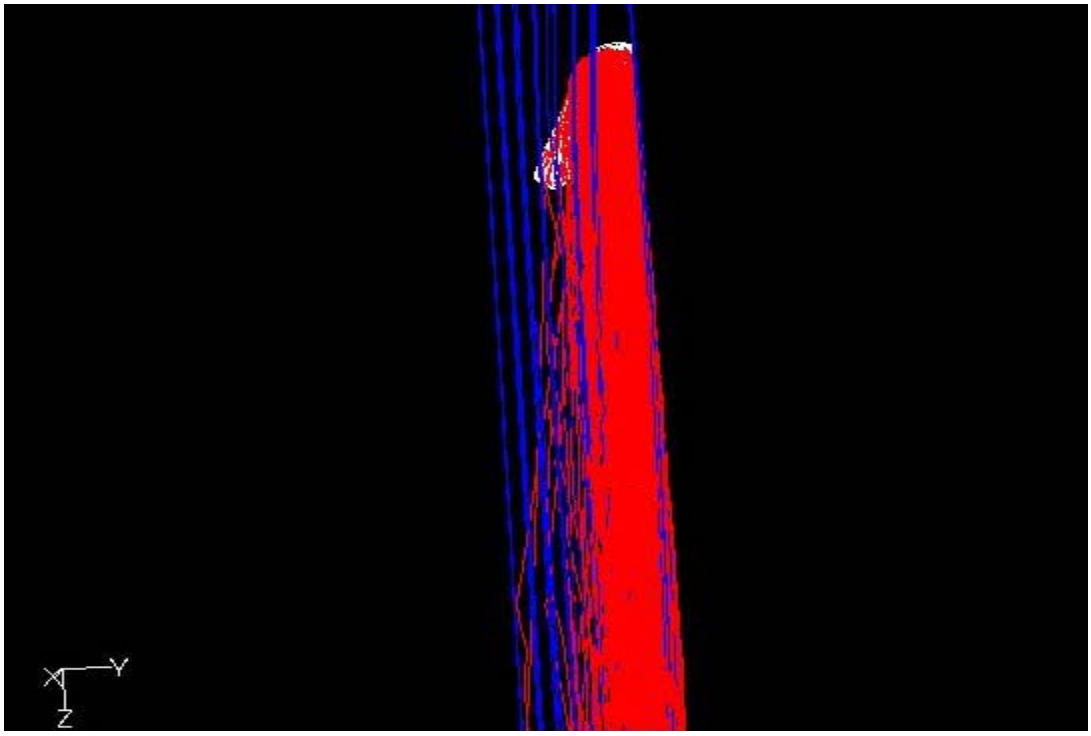

Figure A.7: Particle traces near injection; Red = injection particle, Blue = trace of main flow. r = 0.75, Re_main= 482,820. Re_inj = 99,676. P = 192.4 kPa

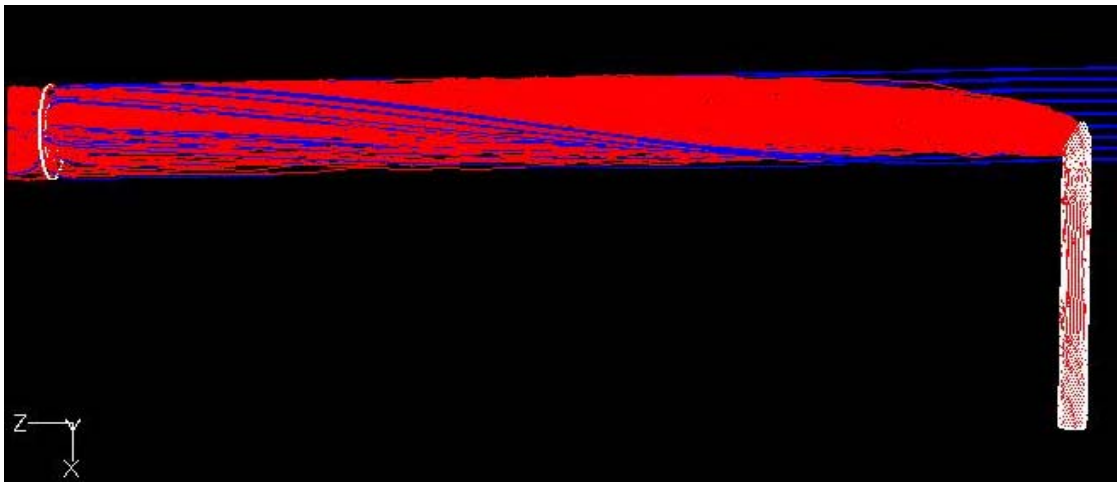

Figure A.8: Particle traces from injection to orifice; Red = injection particle, Blue = trace of pipe walls. r = 1.33, Re_main= 465,297. Re_inj = 176,756. P = 192.4 kPa.

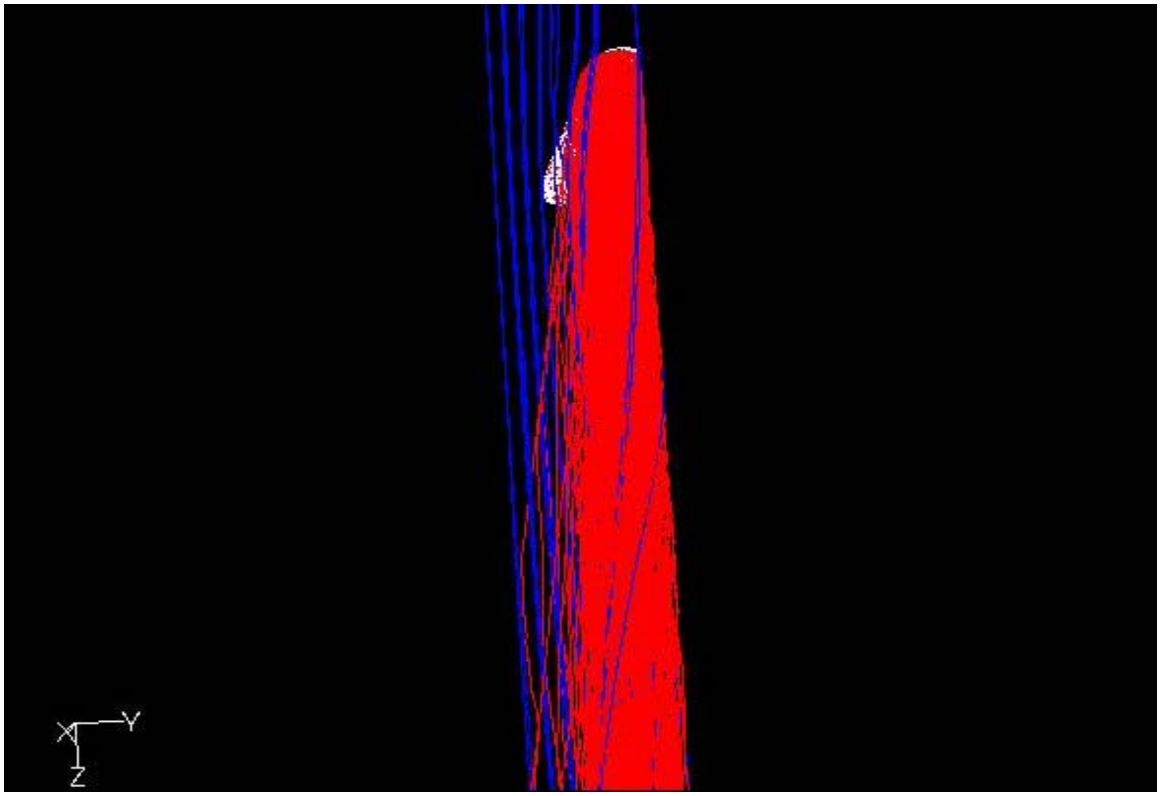

Figure A.9: Particle traces near injection; Red = injection particle, Blue = trace of main flow. r = 1.33, Re_main= 465,297. Re_inj = 176,756. P = 192.4 kPa.

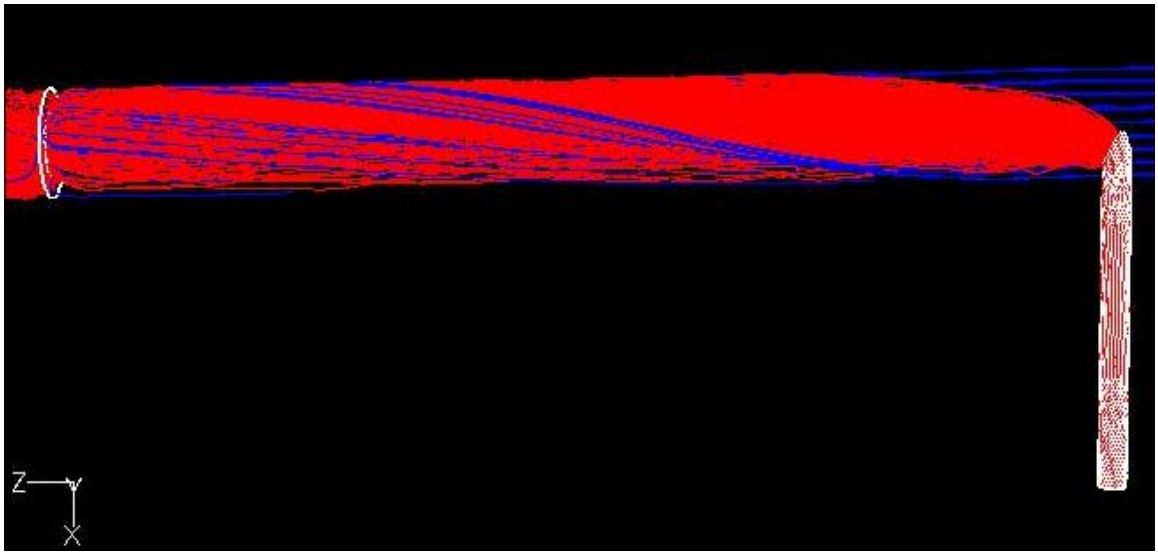

Figure A.10: Particle traces from injection to orifice; Red = injection particle,
Blue = trace of pipe walls. r = 1.50, Re_main= 460,429. Re_inj = 199,360. P = 192.4 kPa.

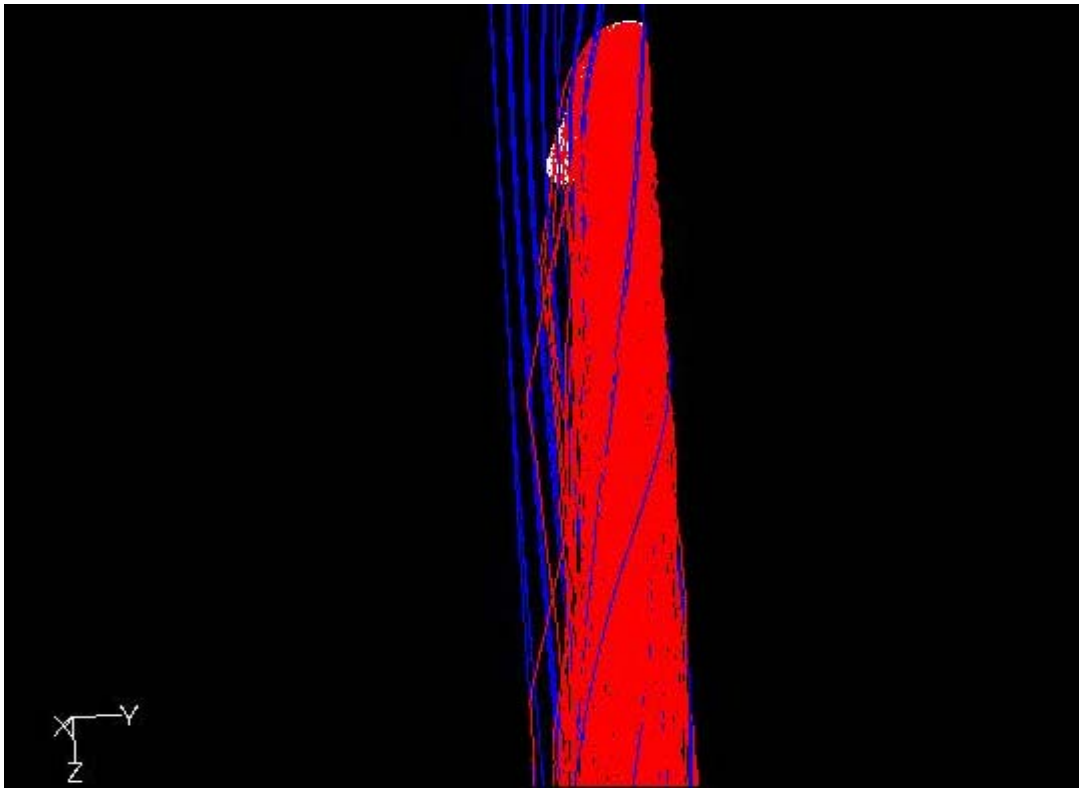

Figure A.11: Particle traces near injection; Red = injection particle, Blue = trace of main flow. r = 1.50, Re_main= 460,429. Re_inj = 199,360. P = 192.4 kPa.

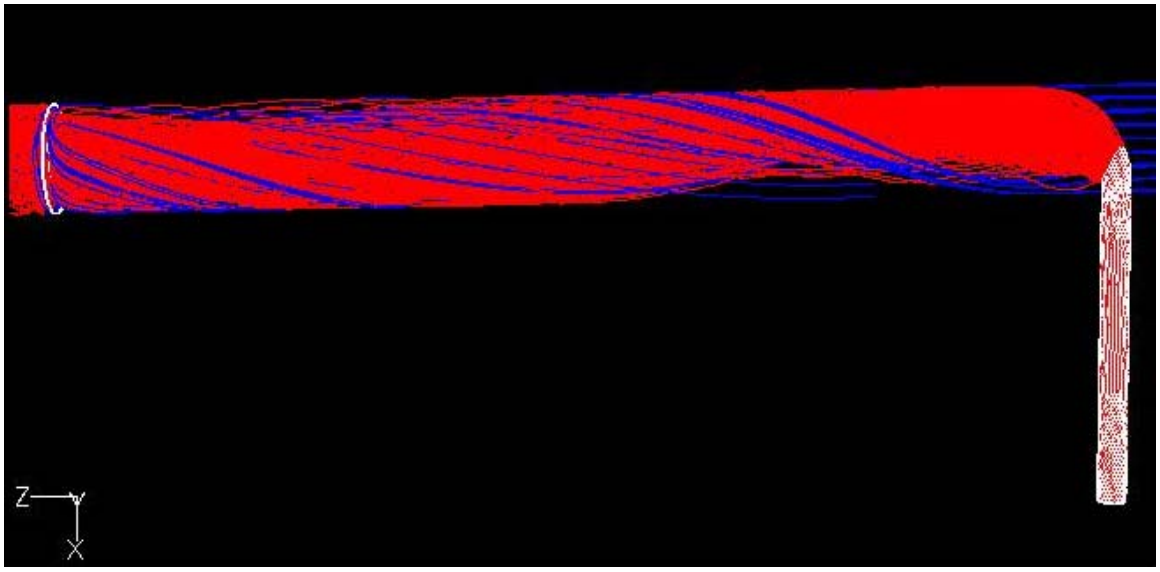

Figure A.12: Particle traces from injection to orifice; Red = injection particle,
Blue = trace of pipe walls. r = 2.25, Re_main= 441,390. Re_inj = 299,054. P = 192.4 kPa.

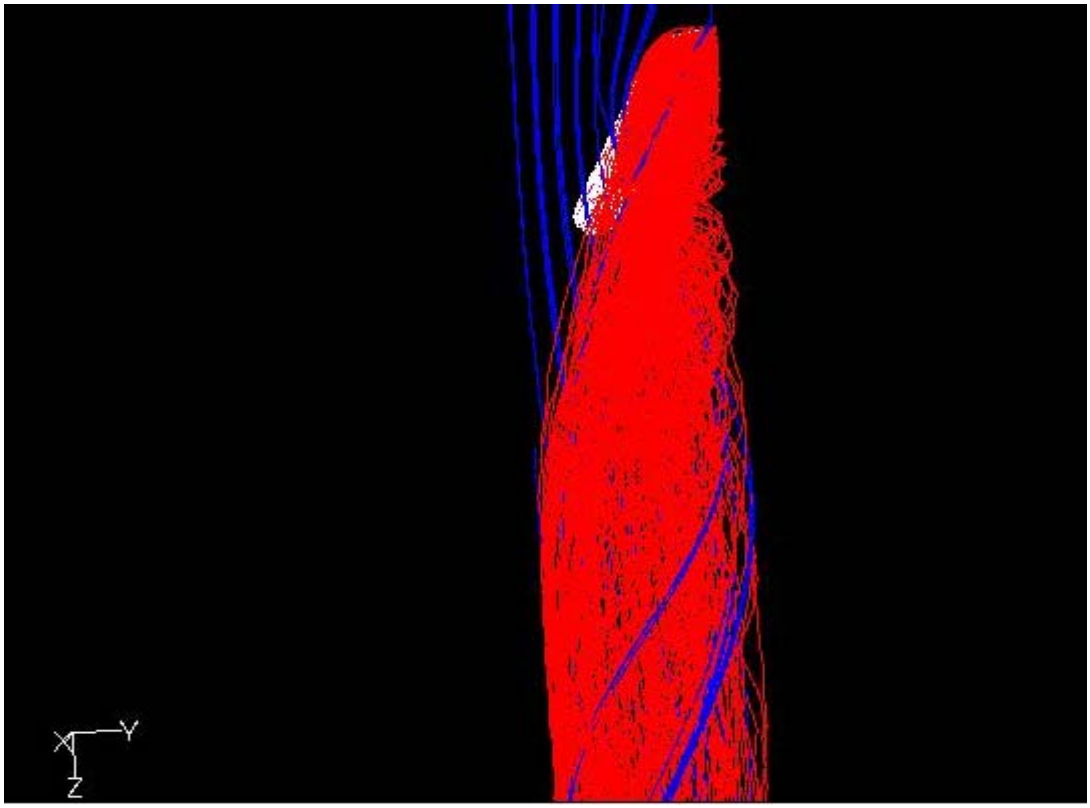

Figure A.13: Particle traces near injection; Red = injection particle, Blue = trace of main flow r = 2.25, Re_main= 441,390. Re_inj = 299,054. P = 192.4 kPa.

Case 3

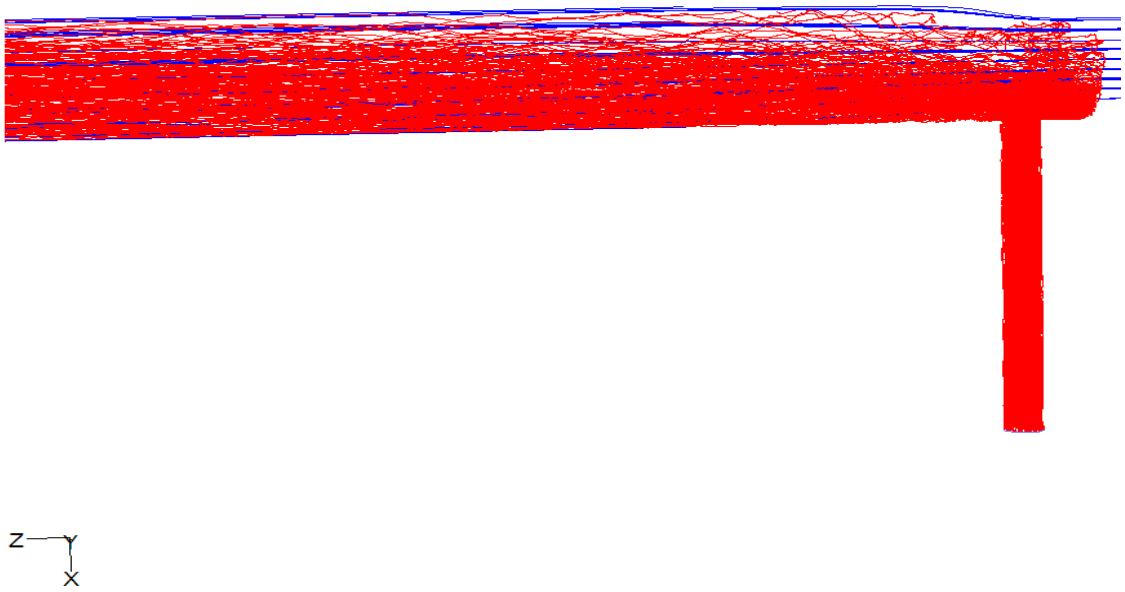

Figure A.14: Particle traces near injection; Red = injection particle, Blue = trace of main flow. r = 0.25, Re_main= 441,390. Re_inj = 33,227. Inlet Pressure = 210 kPa.

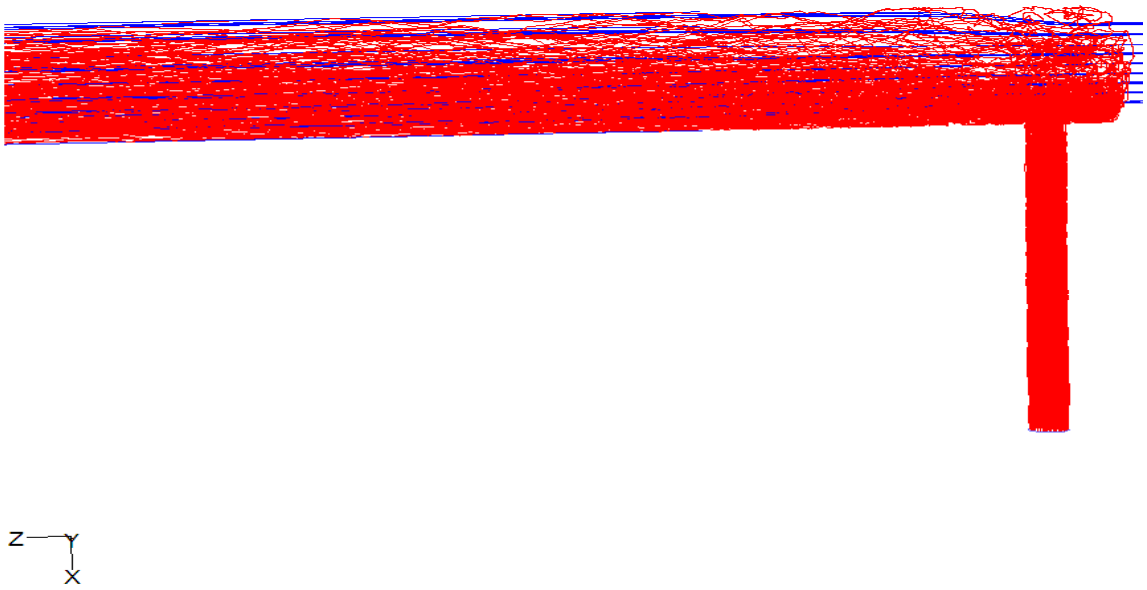

Figure A.15: Particle traces near injection; Red = injection particle, Blue = trace of main flow. r = 0.75, Re_main= 482,820. Re_inj = 99,676. Inlet Pressure = 192.4 kPa.

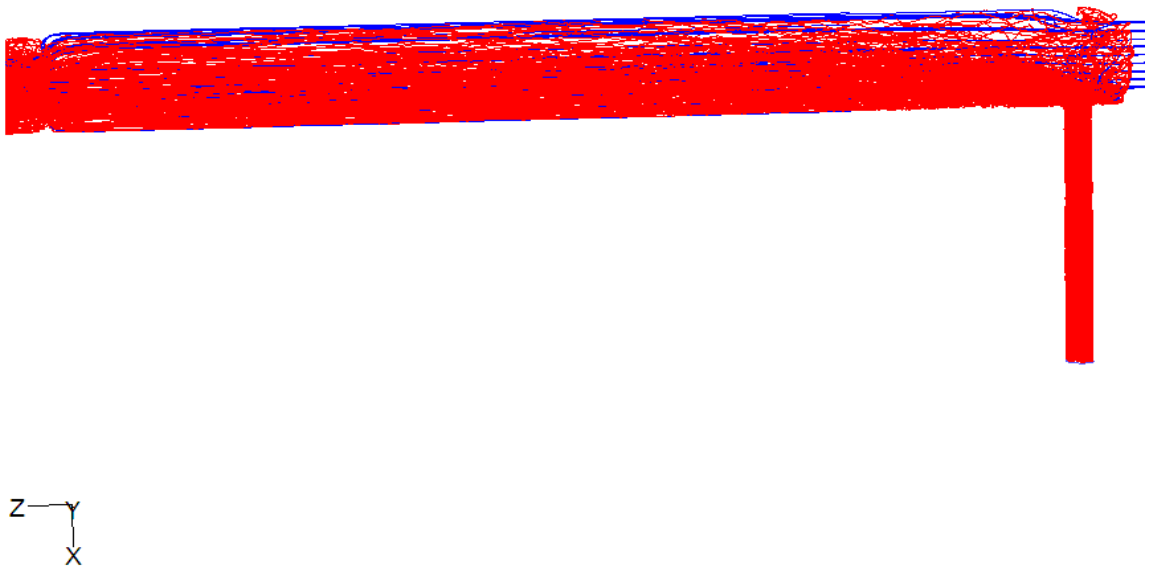

Figure A.16: Particle traces from injection to orifice; Red = injection particle, Blue = trace of pipe walls. r = 1.33, Re_main= 465,297. Re_inj = 176,756. P = 192.4 kPa.

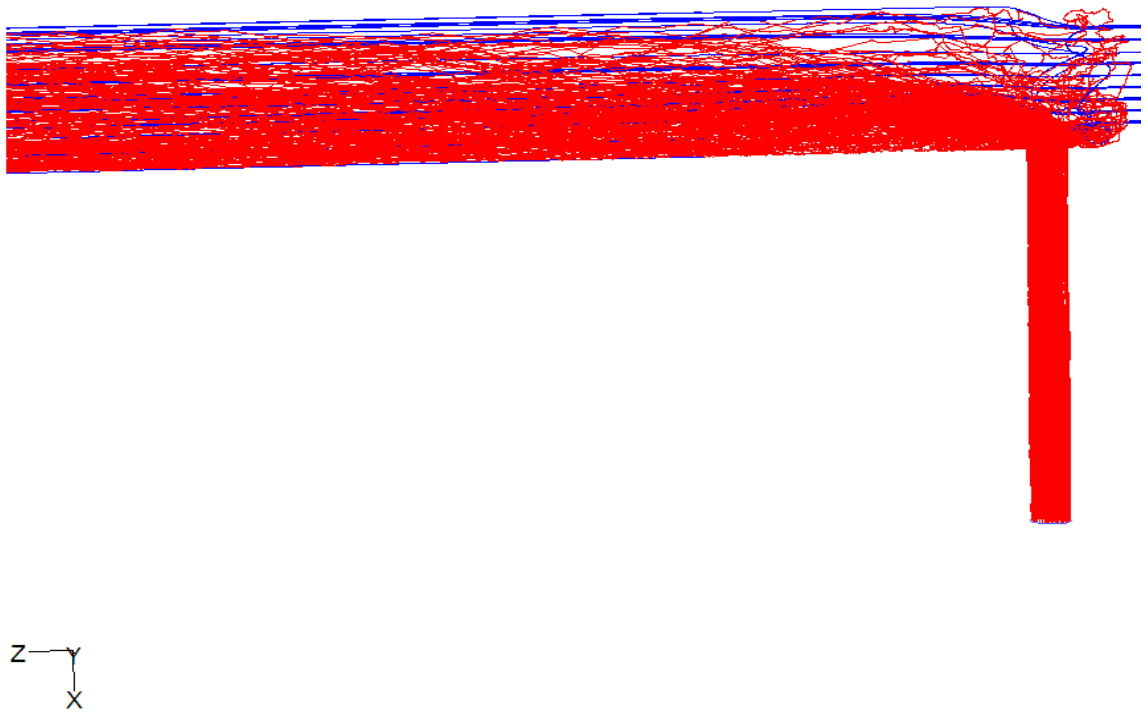

Figure A.17: Particle traces near injection; Red = injection particle, Blue = trace of pipe walls. r = 1.33, Re_main= 465,297. Re_inj = 176,756. Inlet Pressure = 192.4 kPa.

Case 4

Figure A.18: Particle traces near injection; Red = injection particle, Blue = trace of main flow. r = 1.33, Re_main= 465,297. Re_inj = 176,756. P = 210 kPa.

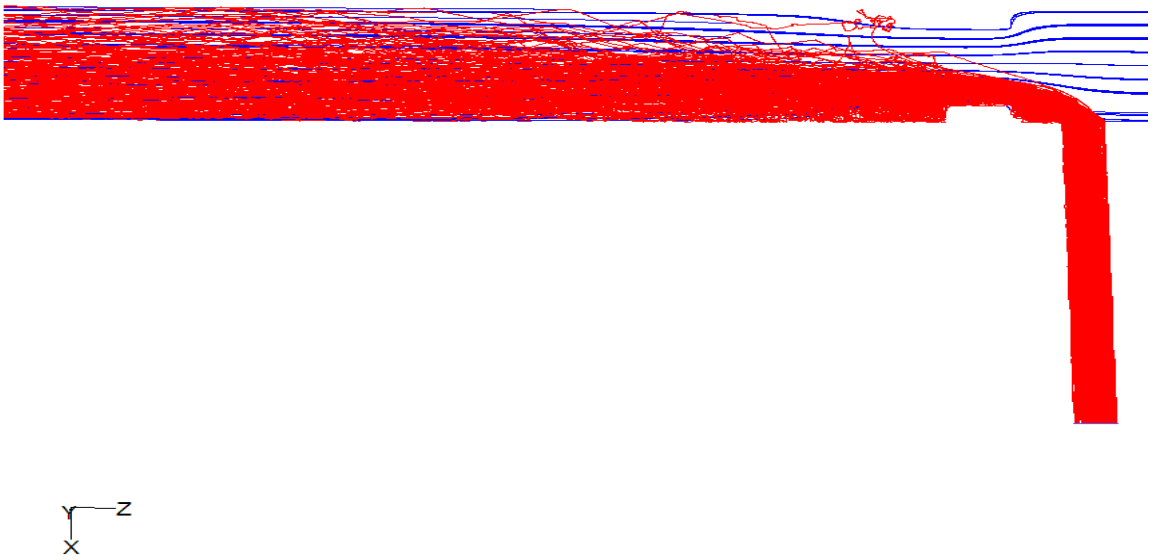

Figure A.19: Particle traces near injection; Red = injection particle, Blue = trace of main flow. r = 0.75, Re_main= 482,820. Re_inj = 99,676. P = 210 kPa.

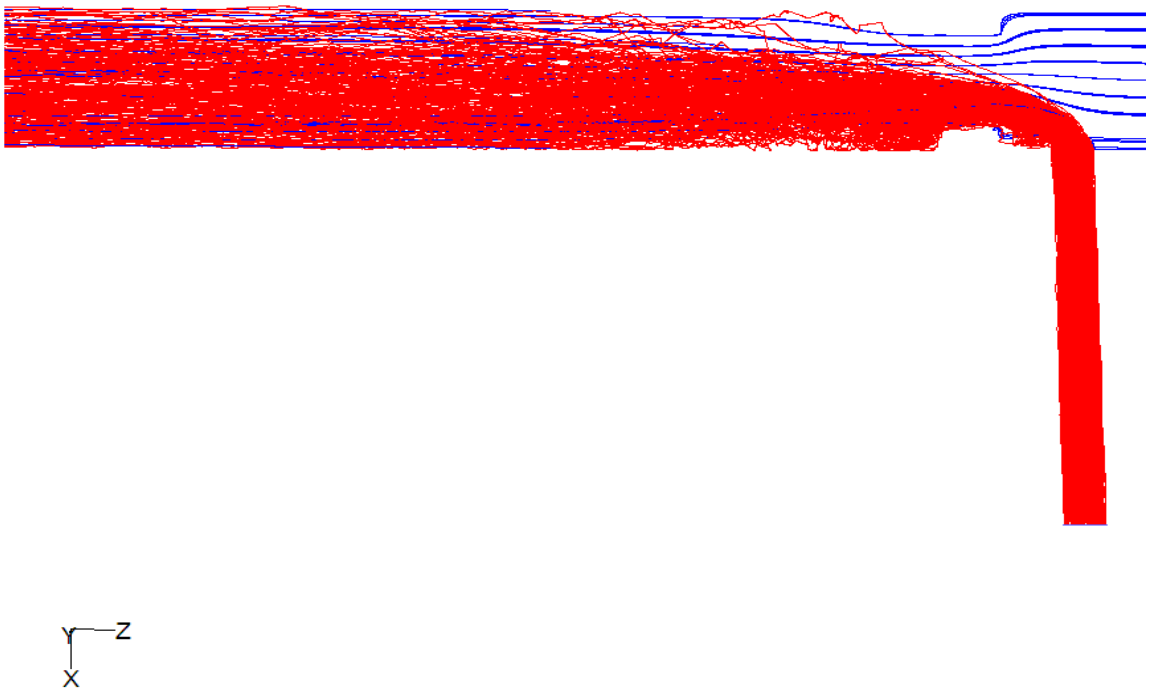

Figure A.20: Particle traces near injection; Red = injection particle, Blue = trace of main flow. r = 0.25, Re_main= 441,390. Re_inj = 33,227. Inlet Pressure = 210 kPa.

REFERENCES

Begemann, Ulrich, and Scherb, Thoroe. "Mixing System for Mixing Two Liquids at Constant Mixture Volume Flow for Supplying Headbox of a Paper Machine." U.S. Patent 5316383. 31 May 1994.

Bertrand, J., Duquenne, A.M., Etcheto, L., and Guirand, P., "Numerical Simulation of In-Line Mixers," European Federation of Chemical Engineers, vol. 17, pp. S511-S516, 1993.

Busko, Michael Jr., and Cozewith, Charles. "Design Correlations for Mixing Tees," Industrial Engineering Chemical Research, vol. 28, pp. 1521-1530, 1989.

Chorin, A.J. "Numerical solutions of navier-stokes equations." Mathematics of Computation. vol 22: pp.745-762, 1968.

Fluent. *Fluent 6.3 UDF Manual*. Fluent Inc., Centerra Resource Park, 10 Cavendish Court, Lebanon, NH, January 2006.

Forney, L.J. and Gray, G.E., "Optimum Design of a Tee Mixer for Fast Reactions," AIChE Journal, vol. 36, no. 11, pp. 1773-1776, November, 1990.

Forney, Larry J. and Louis A. Monclova, "*Numerical Simulation of a Pipeline Tee Mixer*," Industrial Engineering Chemical Research, vol. 34, pp. 1488-1493, 1995.

Forney, L.J. and Sroka, L.M. "Fluid Mixing with a Pipeline Tee: Theory and Experiment," AIChE Journal, vol. 35, no. 3, pp. 406-414, March, 1989.

Kemilainen, I., Kirvesmäki, J., Lappi, J., Turpeinen, H."Apparatus in Connection with a Headbox of a Paper Machine or Equivalent." U.S. Patent 7485206. 3 February, 2009.

Khokhar, Zahid, Sharma, Rajendra, and Zughbi, Habib D. "Mixing in Pipelines with Side-Tees," 6th Saudi Engineering Conference, vol. 2, 171-182, December, 2002.

Launder, B.E., and Spalding D.B. Lectures in Mathematical Models of Turbulence. London, England. Academic Press. 1972.

Meng, Hui, and Pan, Gang. " Experimental Study of Turbulent Mixing in a Tee Mixer Using PIV and PLIF," AIChE Journal, vol. 47, no. 12, pp. 2653-2665, December, 2001.

Pope, Stephen B. Turbulent Flows. Cornell: Cambridge University Press, 2000.